2023

Enhancing Nitrogen Use Efficiency Through Ai-Powered Image Analysis and Innovative N-Rich Spot Method

Bobby Azad
South Dakota State University, bobby.azad@jacks.sdstate.edu

ENHANCING NITROGEN USE EFFICIENCY THROUGH AI-POWERED IMAGE ANALYSIS AND INNOVATIVE N-RICH SPOT METHOD

BY

BOBBY AZAD

A thesis submitted in partial fulfillment of the requirements for the

Master of Science

Major in Plant Science

South Dakota State University

2023

THESIS ACCEPTANCE PAGE
Bobby Azad

This thesis is approved as a creditable and independent investigation by a candidate for the master's degree and is acceptable for meeting the thesis requirements for this degree. Acceptance of this does not imply that the conclusions reached by the candidate are necessarily the conclusions of the major department.

Ali Mirzakhani Nafchi
Advisor Date

David L. Wright
Department Head Date

Nicole Lounsbery, PhD
Director, Graduate School Date

I dedicate this work to my wife Amanda, my parents, and my brothers, whose enduring support and belief in my aspirations have been the bedrock of my journey. Their patience and love provided the strength I needed through this academic venture. To them, I owe a debt of gratitude that words alone cannot express.

"In the symphony of achievement, the quietest whispers of support are the most melodious notes that fuel the soul's crescendo."

Bobby Azad

ACKNOWLEDGEMENTS

I express my deepest gratitude to my supervisor, Dr. Ali Mirzakhani Nafchi, whose guidance and unwavering support have been fundamental to my research. I am also thankful for the valuable insights provided by my committee members, Dr. Reese and Dr. Won. My special appreciation goes to Charlie Edinger, Jack Ingemansen, Dr. Sunish Kumar, Yashar Asgarzadeh, Ahmed Abdalla, Karishma Kumari, and Salman Mirzaee, for their contributions and valuable help. I acknowledge South Dakota State University and the Plant Science Department for the GRA position opportunity and providing the necessary facilities and support during my study. Last but not least, we are grateful for the financial support from the South Dakota Wheat Commission and the U.S. Department of Agriculture.

CONTENTS

ABBREVIATIONS

AE	Agronomic Efficiency
AI	Artificial Intelligence
APE	Agro-physiological Efficiency
ARE	Apparent Recovery Efficiency
BNI	Biological Nitrification Inhibition
CEC	Cation Exchange Capacity
FoV	Field of View
GIS	Geographic Information System
GPS	Global Positioning System
GSD	Ground Sample Distance
HRR	Historical Recommendation Rate
IoU	Intersection over Union
K	Potassium
KML	Keyhole Markup Language
N	Nitrogen
N-rich	Nitrogen-rich
NIR	Near-Infrared
NIRS	Near-Infrared Spectroscopy

NUE	Nitrogen Use Efficiency
OM	Organic Matter
P	Phosphate
PAN	plant-available N
PE	Physiological Efficiency
R-CNN	Region-based Convolutional Neural Network
RE	Recovery Efficiency
SDSU	South Dakota State University
SSM	Site-Specific Management
UAV	Unmanned Aerial Vehicle
UE	Utilization Efficiency
VRA	variable rate application

LIST OF FIGURES

LIST OF TABLES

ABSTRACT

ENHANCING NITROGEN USE EFFICIENCY THROUGH AI-POWERED IMAGE ANALYSIS AND INNOVATIVE N-RICH SPOT METHOD

BOBBY AZAD

2023

This study conducted in 2023 aimed to enhance nitrogen use efficiency (NUE) in wheat and corn grown in South Dakota. Based on dynamic weather conditions and other factor interactions, conventional nitrogen (N) recommendations need to be improved. Soil properties information, including electrical conductivity, was used to create management zones. In each zone, three N-rich spots were established as biosensors. Drones and satellites collected imagery data, and an AI-driven approach assessed the crop response to applied N. A dynamic N application approach, integrating aerial data with historical records, was developed and evaluated. Our methodology, at a 95% confidence level, resulted in a 12.4% higher yield in wheat and a potential 4.77% increase in corn yield compared to conventional approaches, with a 16.2% and 10% reduction in N application in wheat and corn fields, respectively. This led to cost savings and environmental benefits. The financial outcomes revealed cost savings of $7.87 per acre in wheat and $3.62 per acre in corn. The wheat yield increased to 75.09 bu/ac compared to 66.61 bu/ac in control plots, generating an additional revenue of $57.82 per acre. The corn yield increased to 173.75 bu/ac compared to 165.84 bu/ac, indicating a potential increase of 6.89 bu/ac and additional revenue of approximately $34.11 per acre. Moreover, there was a 16.2% increase in NUE in wheat and a 4.3% improvement in corn compared to traditional methods. The findings from this study will be applicable for farmers as a decision-making tool, providing a straightforward approach to enhance NUE while increasing their farm profit.

1 Introduction

1.1 Background of the problem

Throughout history, agriculture has shaped societies, influencing global economic development and societal evolution, beyond providing sustenance [29]. The growing global population created a demand for innovative approaches in the expanding industry [120]. The inception of Precision Agriculture integrates technology with traditional farming to boost crop yields and uphold environmental sustainability [72]. Wheat and corn play a crucial role in global agriculture, transcending cultural and geographical boundaries [99], [106]. They are essential for meeting dietary needs, providing calories, and essential nutrients [15]. Additionally, these grains are widely used in animal feed, biofuels, bioplastics, and various industries [93], [107], highlighting their indispensable role in the global economy. In wheat and corn crop, one of the primary hurdles in maximizing their yield and quality is the efficient and sustainable use of nitrogen. However, the goal is not to minimize nitrogen application, but to find the optimum rate for plant uptake. Figure 1.1 provides a visual representation of this principle. From the leftmost to the rightmost illustration, as the application of nitrogen increases, the yield correspondingly rises. Yet, as Figure 1.2 represent, there is a critical point where, even with additional nitrogen, the yield reaches a plateau. This halt in growth signifies a stage where plants become limited by the availability of other essential nutrients. Thus, over-applying nitrogen past this point does not enhance plant growth. Instead, it can lead to wasted resources, economic drawbacks, and various environmental repercussions such as water body eutrophication, greenhouse gas emissions, and groundwater contamination.

The excessive nitrogen application depicted in Figure 1.2 underscores the need for precision in managing nutrients, especially as we face a growing global population. By 2050, the expected rise to 9.7 billion people will require more efficient nitrogen use to boost crop yields and secure food supply, particularly for key staples like wheat and corn

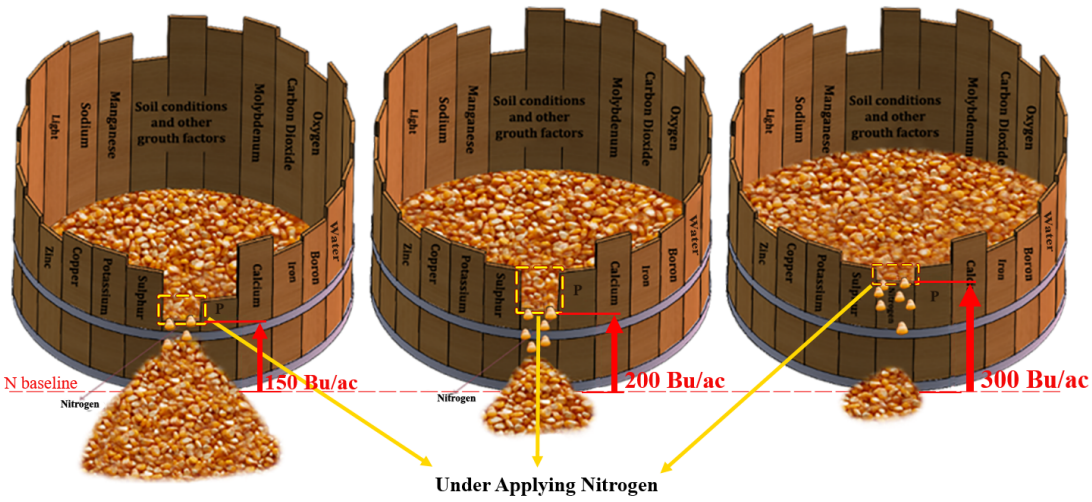

Figure 1.1: Balancing plant nutrient needs. This visual illustrates the relation between increased nitrogen application and yield, emphasizing the critical point beyond which other nutrients limit growth.

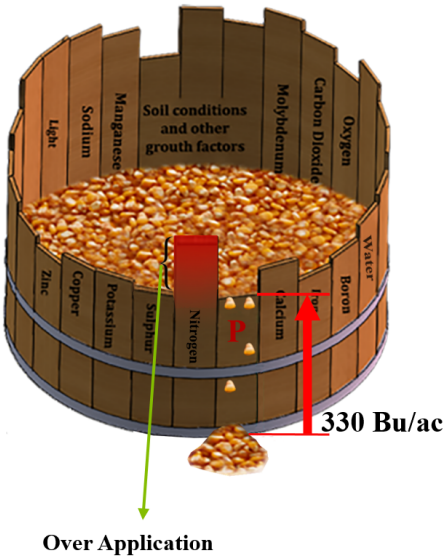

Figure 1.2: Plant growth is limited by various factors; excessive nitrogen fails to enhance growth and leads to economic costs and environmental risks.

[75]. Additionally, with climate change affecting the nitrogen cycle, innovative and adaptable nitrogen management strategies become crucial [22]. These approaches will ensure steady crop production and help maintain a balance between meeting food demands and protecting the environment [109].

Reflecting on the importance of efficient nitrogen management, the practices of

U.S. corn growers from 2013 to 2019 provide a clear example. They applied an average of 92 lbs. of nitrogen per acre annually from manure [115]. Reducing the unnecessary portion of this nitrogen application to match plant needs without excess can bring significant benefits. This adjustment aligns with the goals of sustainable farming practices from both economic and environmental perspectives [105].

1.2 Statement of the problem

Nitrogen's role in agriculture has given rise to challenges that span economic, environmental, and societal dimensions. Beyond the immediate economic and environmental impacts, the broader implications on global food provision and sustainability cannot be overlooked [45].

- **Economic Issues:**
  - Steady rise in nitrogen fertilizer prices.
  - Financial strain on small and medium-sized farms.
  - Increased consumer food prices impacting food security and widening socioeconomic disparities.
- **Environmental Challenges:**
  - Volatilization leading to air pollution.
  - Denitrification resulting in release of nitrous oxide, a potent greenhouse gas.
  - Eutrophication in water bodies causing harmful algal blooms.
- **Societal Implications:**
  - Global food supply at risk due to rising costs leading to inefficient fertilizer use.
  - Impact on fisheries from eutrophication, affecting protein sources.

- Weather unpredictability, intensified by global warming, threatens consistent food provision.

In essence, a holistic approach, integrating agronomy, soil science, economics, and environmental knowledge, is crucial to address these multifaceted challenges surrounding nitrogen use in agriculture.

1.3 Advancements in precision agriculture and technology integration

Modern agricultural practices have embraced a blend of both innovative techniques and technological advancements. Specifically, these include precision agriculture tools like Site-Specific Management (SSM), variable rate nitrogen application, and ramp application, as well as cutting-edge technologies like Artificial Intelligence (AI) and remote sensing. These tools and technologies aim to optimize nitrogen application, enhancing both its economic and environmental efficiencies.

1.4 Site-specific management

The first approach to address the challenges of nitrogen usage is adopting SSM, a prospective solution tailored to specific demands of varied agricultural zones. It emphasizes managing agricultural inputs, such as water, seeds, and fertilizers, on a site-specific basis [78]. By understanding the spatial variability within a field, which arises from variations in soil properties, topography, and other microclimatic factors, SSM offers a refined method to optimize resource use, streamline costs, and enhance productivity. Importantly, this strategy aims at curtailing the environmental footprint of farming practices [94].

Instead of using a uniform application of nitrogen fertilizer across an entire field, SSM and variable rate application enables farmers to customize the amount of fertilizer used based on the specific requirements of different field sections. This is usually determined through advanced technologies, like soil conductivity mapping, remote

sensing, and Geographic Information System (GIS), which can provide detailed and precise information about the spatial variability of nutrient requirements within a field [14].

Variable rate nitrogen application revolutionizes the traditional fertilizer process, aligning the nitrogen supply directly with crop needs, thereby enhancing Nitrogen Use Efficiency (NUE) and reducing environmental impacts, including nitrogen leaching and atmospheric emissions [84]. This approach not only optimizes yields but also bolsters farm profitability by efficiently allocating resources, leading to reduced fertilizer costs and improved crop returns [92], [108]. SSM, with strategies like variable rate application, exemplifies a sustainable, data-driven farming method that marries economic benefits with environmental responsibility [102].

1.5 Nitrogen-rich strip and ramp application

After exploring SSM and its specialized strategies, we now transition to other techniques that address nitrogen use challenges. The Nitrogen-rich (N-rich) strip and the ramp application are the methods offer distinct approaches to assessing in-season nitrogen needs, ensuring timely and efficient application in diverse agricultural contexts.

The Nitrogen-rich strip provides an overview of the field's nitrogen requirements by covering an extensive area. The expansive nature of the strip allows for an enhanced understanding of the variability in nitrogen needs across the field.

The ramp application adjusts nitrogen fertilizer applications based on the specific growth stages of crops. This approach focuses on the temporal dimension, ensuring that crops receive the right amount of nitrogen when they need it most. Instead of applying nitrogen uniformly throughout the crop's life cycle, the ramp application tailors the amount and timing to coincide with crucial growth phases, thereby optimizing nitrogen absorption. Tools like the GreenSeeker, which quantifies plant greenness, offer a more objective and reliable measure for estimating a plant's nitrogen uptake.

1.6 Technological solutions

While tailored agricultural strategies such as N-rich strip and ramp applications lay the groundwork for optimized nitrogen usage, the merger of AI and remote sensing technologies augments their reach. These modern tools herald a transformative approach to surmounting the challenges associated with nitrogen use in agriculture, especially when supplementing traditional strategies [33]. An epitome of these technological advancements is deep learning models, like the Faster R-CNN (Region-based Convolutional Neural Network) model [40], which has displayed proficiency in various applications.

The Faster R-CNN, an exemplary object detection algorithm, is particularly pivotal for our study. While GPS data offers invaluable localization in aerial imagery, it occasionally grapples with inconsistencies. In contrast, the Faster R-CNN can detect and pinpoint objects within aerial images. In this research, these detected objects, become reference markers, notably the tiled areas mentioned in section 3.3.

Furthering our technological arsenal, we amalgamate the AI-driven image analysis powered by Faster R-CNN with other remote sensing instruments. Satellite imagery, particularly from sources like Sentinel, harmonizes with our AI techniques, accentuating the granularity and acuity of our conclusions. Such a holistic approach epitomizes the synergistic potential of AI and remote sensing in pioneering precise nitrogen management strategies.

This section primarily provides a glimpse of the Faster R-CNN model's significance. The ensuing methodology chapter will delve deeper into its nuances, juxtaposed with other technological instruments and methods.

1.7 Research questions

The complexity nature of nitrogen application in agriculture and the advent of technological and strategic advancements, this research aims to answer the following

questions:

- **NUE through precision agriculture:** what specific strategies and tools in precision agriculture are most effective in enhancing the NUE of wheat and corn?
- **Optimization of nitrogen-rich areas:** how can the identification and management of areas with elevated nitrogen levels be utilized to effectively measure plant responses to varied nitrogen concentrations?
- **Bio-sensing efficacy:** how effective is the N bio-sensing system in maintaining crop yields while conserving nitrogen, and what are its broader impacts on economic, environmental, and societal dimensions?
- **In-season monitoring:** in what ways can AI-driven image processing, as opposed to traditional practices, contribute to in-season and precise monitoring of crop conditions for optimal nitrogen application?
- **Advanced image processing:** how do advanced, AI-based image processing techniques compare to basic methods in terms of accuracy and depth of analysis for agricultural needs?
- **AI and remote sensing synergy:** how does the integration of AI with remote sensing tools, such as drones and satellites, offer advantages over standalone methodologies in understanding and managing crop nitrogen needs?
- **AI-Driven nitrogen application system:** how can AI-driven systems, incorporating advanced image processing techniques, optimize variable rate nitrogen application, and how do these systems compare to traditional practices?
- **AI tailoring:** how can AI models, specifically tailored for agriculture, improve the accuracy and efficacy of nitrogen management when compared to generic AI models?

- **Data integration and analysis:** how does consolidating data from diverse sources like drone imagery, satellites, and historical records provide enhanced insights into nitrogen application strategies over traditional singular data sources?

1.8 Purpose of the study

This study aims to improve NUE in wheat and corn production in US, a path toward sustainable and resilient farming systems. Improvement of NUE can enhances crop yield and quality, addressing global food demands, and has the potential to alleviate environmental issues related to excessive nitrogen use, such as water eutrophication and increased greenhouse gas emissions

This research focuses on the role of technology in improving NUE in wheat and corn production. By applying Precision Agriculture and Site-Specific Management techniques, such as variable rate nitrogen application and soil conductivity mapping, along with advanced tools like remote sensing, image analysis, and AI, the study aims to create a more precise, sustainable, and environmentally friendly agricultural system.

1.9 Research locations

This study was conducted in South Dakota, United States, focusing on wheat and corn crops. It encompassed a 3.36-acre plot at the South Dakota State University (SDSU) Agricultural Experiment Station in Brookings for wheat trials and a 135.54-acre on-farm research site for corn in Mount Vernon, SD. In both fields, the preceding crop was soybean, setting a consistent pre-cultivation condition for our research. While this chapter introduces our research locations. Detailed discussions on soil features and relevant data will be in Chapter 4.

1.10 Organization of this thesis

The organization of this thesis is structured to provide a logical flow of information and analysis. The chapters are organized as follows:

Chapter 1: Introduction This chapter presents a broad overview of the research topic, delineating the background and statement of the problem, research questions, and the purpose of the study. The chapter serves as a roadmap to the thesis, setting the stage for the subsequent in-depth analysis and discussion.

Chapter 2: Literature Review In this chapter, we offer a review of existing literature on factors influencing NUE and the potential of SSM in improving NUE. This systematic review will provide a robust understanding of the current state of knowledge and reveal gaps that this study aims to address.

Chapter 3: Research Methodology This chapter details the methodological approach adopted in this study. The research design, data collection procedures, and analytical techniques are all meticulously laid out. This will ensure the study's reliability and validity, allowing for the results to be rigorously examined and evaluated.

Chapter 4: Experimental Results In this chapter, we present the findings of the research, analyzed and discussed in the context of the research questions. This examination will offer valuable insights into the factors influencing NUE and the potential of SSM, guiding the recommendations and implications drawn in the final chapter.

Chapter 5: Conclusion The final chapter summarizes the key findings and discusses their practical implications. It also points out potential avenues for future research, providing guidance for both scholars and practitioners.

2 Literature review

2.1 Introduction to the literature review

This chapter builds upon the foundational understanding of nitrogen's role in agriculture, delving into strategies for enhancing NUE and examining the impact of AI and Remote Sensing in modernizing nitrogen management. It aims to integrate traditional agricultural practices with technological advancements, providing a view of current nitrogen management approaches.

2.2 Purpose and scope of the review

This literature review sets out to provide a broad perspective on the existing body of research surrounding nitrogen use in crops such as wheat and corn. Through a critical examination of methodologies, insights, and existing challenges found in prior studies, we aim to contextualize our research endeavors and elucidate their relevance in the larger academic dialogue surrounding nitrogen management.

2.3 Overview of the main themes to be covered

This review traces the development of nitrogen management in agriculture, from early methods to current advanced techniques. It focuses on the evolution of best practices and addresses current challenges. The review also highlights technological advances, especially in remote sensing and AI, like the Faster R-CNN model, which improves the selection of drone images for precise analysis. The impact of these innovations on NUE, particularly for wheat and corn, will be emphasized.

2.4 Nitrogen application in modern agriculture

Building on our previous discussions, it is evident that nitrogen's role in agriculture is multifaceted, bridging both its foundational importance for crop growth and the challenges

tied to its application. As the modern agricultural landscape evolves, the intricacies of nitrogen application must be keenly understood to harness its benefits fully [24].

Predominantly, agricultural systems utilize nitrogen (N) in two primary forms [122]: ammonium $(NH_4{}^+)$ and nitrate $(NO_3{}^-)$. These forms are supplied to crops via bio/chemical fertilizers and organic manure. While these applications are crucial for sustaining crop growth, the art and science of nitrogen application go beyond mere addition to the soil.

The contemporary challenges arise from optimizing the amount, timing, and method of nitrogen application. Over-application or inappropriately timed application can lead to various environmental and economic inefficiencies. In response to these challenges, the agricultural sector has implemented measures like NUE to more effectively assess and improve nitrogen application. NUE stands as a crucial tool in optimizing nitrogen efficiency, addressing both environmental and economic concerns in agriculture.

2.5 An overview of NUE

Modern agriculture seeks to balance the dual objectives of increasing productivity and environmental conservation [9]. NUE is key in this effort, as it measures how effectively crops use nitrogen to grow and yield. This efficiency is vital for both economic viability and environmental sustainability in farming [60]. However, it's crucial to support this definition of NUE with authoritative sources that specifically state its role in quantifying crop growth and yield from nitrogen application. Research underscores NUE's importance in enhancing crop yields and reducing negative environmental impacts of nitrogen loss [59], [61].

NUE comprises two key metrics: Agronomic Efficiency (AE) and Recovery Efficiency (RE) [43]. AE measures the yield increase obtained for each unit of nitrogen applied, essentially reflecting how effectively nitrogen contributes to crop production [44]. It is a critical measure for understanding how nitrogen application translates into actual

yield gains. On the other hand, RE quantifies the proportion of applied nitrogen that is actually absorbed and utilized by the crop. This metric is important for assessing how much of the applied nitrogen is being taken up by the plant, as opposed to being lost to the environment. Together, AE and RE provide a comprehensive picture of nitrogen's role in crop yield and its utilization efficiency [19], [70].

2.5.1 Assessing NUE: different perspectives

Traditionally, NUE is determined by the ratio of crop yield (Y) to nitrogen inputs (N), as depicted in Equation 2.1:

$$NUE = \frac{Y}{N} \tag{2.1}$$

However, this formulation has provoked scholarly debate due to the varied interpretations of 'yield.' Fageria and Baligar [34] proposed multiple methodologies to account for these nuances. The equations below further detail the calculation methodologies for AE, Physiological Efficiency (PE), Agro-physiological Efficiency (APE), Apparent Recovery Efficiency (ARE), and Utilization Efficiency (UE):

$$AE = \frac{Gf - Gu}{Na} \tag{2.2}$$

where (Gf) represents grain yields of the fertilized, (Gu) refers to unfertilized plots, and (Na) shows the applied nitrogen rate (Na).

$$PE = \frac{Yf - Yu}{Nf - Nu} \tag{2.3}$$

This equation uses the total above-ground biomass of the crop in fertilized (Yf) and unfertilized plots (Yu), and the nitrogen contents of the above-ground biomass in the fertilized (Nf) and unfertilized plots (Nu).

$$APE = \frac{Gf - Gu}{Nf - Nu} \tag{2.4}$$

$$ARE = \frac{Nf - Nu}{Na} \tag{2.5}$$

$$UE = \frac{Yf - Yu}{Na} \tag{2.6}$$

As the equations indicate, NUE's interpretation can vary based on the metric in use. The complexity of NUE is further accentuated by innovative definitions such as the "biologically significant" NUE proposed by Berendse and Aerts [12]:

$$\text{Biologically Significant NUE} = \frac{An}{Ln} \tag{2.7}$$

This broader perspective on NUE, while addressing limitations of previous definitions, emphasizes the need to consider external factors like climate change, crop management techniques, and new biotechnologies. It highlights the importance of comprehensive methods that include both native soil plant-available nitrogen (PAN) and potential PAN balances, along with traditional fertilizer inputs. Given the impact of changing climate conditions, such as increased atmospheric CO_2 and temperature, on nitrogen dynamics, a deeper understanding of NUE is crucial. This involves exploring genetic, physiological, and environmental influences on NUE and developing innovative strategies to improve it.

2.5.2 Factors influencing NUE

NUE is a complex subject; however, four key elements are of particular importance: the type of soil, climate conditions, the variety of crop, and the site-specific management strategies [32], [44], [60].

Firstly, it is essential to consider that the various characteristics of the soil, Soil texture, organic matter content, electrical conductivity, pH and so on are all crucial determinants in understanding NUE. The reason is that significantly influences of soil properties on the bioavailability and potential loss of nitrogen [79]. More specifically, the soil texture impacts the way in which water and nitrogen move through the soil profile. Fine texture soils for example loamy and clay soil retain nitrogen more effectively than sandy soils. In the last soil, nutrients can be more easily leached away. The soil organic matter can also determine soil nitrogen amount and availability for crop [65]. Higher organic matter content often leads to a greater nitrogen supply. Finally, the soil pH plays a vital role in dictating nitrogen chemical states in soil solution, affecting its availability for crop. Therefore, soil characteristics can effectively determine the NUE [32], [42].

Climate factors, especially precipitation and temperature, are another crucial group of factors influencing NUE [69]. These environmental parameters not only affect the loss of nitrogen via various processes such as volatilization, leaching, and denitrification but also directly impact the nitrogen uptake ability of crops. For example, high rainfall levels can lead to increased nitrogen leaching, while extremely high or low temperatures can inhibit biological nitrogen fixation and uptake by crops. Therefore, understanding the climatic influences can offer valuable insights into the ways of improving NUE [39], [60].

Agronomic management strategies also play a pivotal role in determining NUE. For example, right source, right rate, right place, and right time of nitrogen application as agronomic management strategies can influence the NUE [118]. For instance, a well-coordinated nitrogen delivery strategy that aligns with the periods of peak plant demand (i.e., right time) can significantly enhance NUE [118]. Timing nitrogen application to coincide with critical growth stages can help maximize crop uptake and reduce losses to the environment. Similarly, choosing the right place and rate of application can also make a considerable difference. For example, with practices like split application and use of controlled-release fertilizers can be a beneficial strategy for

optimizing NUE [43].

Lastly, the specific genotype of the crop is an integral part of the NUE equation [67]. This involves the crop's inherent efficiency in nitrogen uptake, assimilation, and remobilization. Crop genotypes vary in their ability to absorb nitrogen from the soil, assimilate it into organic forms, and remobilize it to the grains during the reproductive stage. Thus, plant breeding and genetic improvement programs can contribute significantly to enhancing NUE, offering a sustainable and long-term approach to improve nitrogen use in agriculture [44].

While the genotype of the crop plays a pivotal role in determining its nitrogen uptake efficiency, it is equally crucial to comprehend the other side of the equation: how nitrogen, once applied, can be lost from the soil. This understanding is paramount because, irrespective of a crop's genetic predisposition to utilize nitrogen efficiently, significant losses from the soil can undermine the overall NUE. By grasping the pathways through which nitrogen escapes, we can devise strategies that not only optimize its use by crops but also minimize its wastage and environmental impact.

2.6 Understanding nitrogen loss pathways

Nitrogen, being a vital nutrient, has a transient nature in the soil [79]. It is susceptible to rapid migration from its application point, leading to losses through several mechanisms. These mechanisms, encompassing processes like nitrification, volatilization, denitrification, leaching, and surface runoff, can have profound impacts on the environment and the economy [8], [101]. Not only do they influence the potential yield and profitability of crops, but they also pose threats to ecosystems, water resources, and the health of animals and humans.

The nitrogen balance equation, represented by Equation 2.8, effectively describes the quantity of mineral nitrogen present in the soil at any specific moment [27].

$$N = N_p + N_b + N_f + N_u + N_m - N_{pl} - N_g - N_i - N_l - N_e \tag{2.8}$$

where:

- N_p is the precipitation and dry deposition,
- N_b is the biological fixation,
- N_f is the nitrogen from fertilizer application,
- N_u is the nitrogen return to the soil through urine and dung,
- N_m is the nitrogen from mineralization,
- N_{pl} is the nitrogen taken up by plants,
- N_g is the nitrogen loss through gaseous emissions,
- N_i is the nitrogen loss through immobilization,
- N_l is the nitrogen loss through leaching,
- N_e is the nitrogen loss through erosion and surface runoff.

The nitrogen balance equation provides a holistic view of the various factors influencing the nitrogen content in the soil. However, to truly optimize nitrogen management, it is essential to delve deeper into the specific processes that lead to nitrogen loss. Each of these processes, from nitrification to leaching, plays a unique role in determining how nitrogen moves and transforms within the soil ecosystem. In the following sections, the mentioned pathways are explored in more details, shedding light on their mechanisms, implications, and significance in the broader context of NUE.

2.6.1 Nitrification process

Nitrification is a key microbial process involving two stages, in which ammonium $(NH_4{}^+)$ is oxidized to nitrate $(NO_3{}^-)$ [119]. This process begins with ammonia oxidizing bacteria, specifically Nitrosospira and Nitrosomonas, which oxidize $(NH_4{}^+)$ to nitrite $(NO_3{}^-)$. Subsequently, Nitrobacter bacteria oxidize $(NO_2{}^-)$ to $(NO_3{}^-)$ [51]. Nitrification mainly occurs in well-aerated soil environments with optimal soil moisture levels. The rate of nitrification can be influenced by various factors, including soil temperature, pH, $NH_4{}^+/NH_3$ concentration, and the density of the microbial population [98]. Nitrate produced through nitrification process can be utilized by crops, immobilized by soil microorganisms, or leached from the soil.

2.6.2 Volatilization

Volatilization is a significant pathway of nitrogen loss where ammonium $(NH_4{}^+)$ is transformed into ammonia gas (NH_3), which can then be further converted to atmospheric nitrogen (N2) [55]. This process is principally facilitated by the enzyme urease, which catalyzes the conversion of urea to ammonium and carbon dioxide.

Under alkaline soil conditions, a significant proportion of the ammonium can be lost to the atmosphere as ammonia gas, which can then be transported away by wind currents [17]. As such, mitigating volatilization is particularly crucial in regions where urea-based fertilizers are widely utilized.

2.6.3 Denitrification

Denitrification is an anaerobic microbial process wherein nitrate $(NO_3{}^-)$ is reduced to nitrogen gas (N2) [41]. This reduction involves the formation of intermediate products such as nitrogen dioxide (NO_2), nitric oxide (NO), and nitrous oxide (NO_2) [38], [83]. Notably, the production of (NO_2) is a significant environmental concern due to its potent greenhouse gas potential [41]. The extent of nitrogen loss through denitrification is

influenced by several factors, including soil water content, the availability of soluble carbon, the presence of nitrate, temperature, and the duration of the process [16].

Traditional management strategies aimed at preventing denitrification losses have focused on inhibiting soil nitrification, thereby preventing the formation of nitrate from ammonium [76]. Various chemicals, including nitrapyrin, thiourea, thiophosphoryl triamide, 3,4-dimethyl pyrazole phosphate (DMPP), and dicyandiamide (DCD), are utilized for this purpose [5], [68]. It is worth noting, however, that these compounds can inadvertently increase nitrous oxide production and release from soils. As such, the exploration of Biological Nitrification Inhibition (BNI) strategies, involving both plant-derived compounds and indirect mechanisms, offers promising alternatives to mitigate nitrogen losses [24], [73].

2.6.4 Soil erosion and runoff

Soil erosion and runoff contribute significantly to the global loss of nitrogen, particularly from surface soil that is typically laden with high concentrations of nitrogen and organic matter [53], [64]. This process can be particularly harmful in agriculturally intensive regions where the soil is routinely disturbed and exposed to weather elements, thereby increasing the risk of erosion. The lost nitrogen from soil erosion and runoff not only reduces the fertility of the land but also pollutes downstream water bodies, contributing to eutrophication and diminished water quality [30].

Effective management of cropping systems can substantially curb these losses. Practices such as reduced tillage or no-tillage, cover cropping, contour tillage, terracing, and grassed waterways have been widely recommended [13], [35]. Reduced tillage and no-tillage practices, for instance, minimize the disruption of soil, preserving its structure and reducing [95]. On the other hand, cover cropping enhances the soil organic matter content, thereby improving its structure, increasing its water holding capacity, and decreasing runoff [25].

Cover crops also enhance NUE through various mechanisms [47]. These include reducing soil erosion, fixing atmospheric nitrogen into plant-available form, and scavenging nitrogen from soils to prevent leaching [26], [85]. Through these actions, cover crops not only retain the soil fertility but also mitigate the environmental impacts associated with nitrogen losses.

2.6.5 Nitrogen mineralization and immobilization

Nitrogen mineralization, the microbial-mediated process that transforms organic nitrogen forms into inorganic forms, mainly ammonium $(NH_4{}^+)$, plays an essential role in the nitrogen cycle. This process, influenced by various biotic and abiotic factors, plays a key role in making nitrogen available in forms that plants can utilize [20]. However, the mineralization process is not always beneficial for the plant nitrogen supply, particularly when the carbon to nitrogen (C:N) ratio of the organic matter is high (e.g., ¿30:1) [48].

Under such conditions, mineralization is inhibited due to insufficient nitrogen content, and a process known as nitrogen immobilization dominates instead. Immobilization is a phenomenon where soil microorganisms, requiring nitrogen for protein synthesis and reproduction, incorporate nitrogen into their biomass, thereby reducing plant-available nitrogen [80], [121]. As a result, the short-term supply of nitrogen to plants can be negatively impacted.

Although nitrogen immobilization initially reduces the availability of nitrogen to plants, this does not mean the nitrogen is permanently removed from the soil ecosystem [77]. Over time, immobilized nitrogen can re-enter the cycle through microbial activities. As microbes die and decompose, the nitrogen within their biomass becomes available again, a process referred to as remineralization [123]. This remineralization is a key aspect of the soil's nitrogen cycle, where dead microbial biomass is broken down, releasing nitrogen back into the soil in forms accessible to plants. This dynamic interplay between immobilization and remineralization ensures a continual, albeit fluctuating,

supply of nitrogen within the soil system [100].

2.6.6 Leaching

The overuse of animal manure or nitrogen fertilizers can significantly intensify the leaching of nitrate (NO_3^-), especially following an upsurge in the concentration of available N within the soil solution [63]. Nitrate is highly prone to leaching because its negative charge prevents it from associating with the negatively charged soil colloids. Conversely, ammonium (NH_4^+) is electrostatically bound to colloids, making it resistant to leaching [113].

Rainfall and irrigation can effectively wash out nitrate from the system, exacerbating its loss [57]. This loss is most significant during periods of heavy rainfall and during periods of slow crop growth when the plant nitrogen uptake is reduced [49]. As a result, leaching is a significant contributor to the global loss of nitrogen from soils, accounting for an estimated 2%–60% of applied nitrogen [49].

Studies on irrigated wheat fields in Northern Mexico, where farmers apply 250 kg N ha^{-1} in two split applications, estimated the nitrogen loss through leaching to be between 5 and 12.5 kg N ha^{-1} [91]. It is noteworthy that the texture and structure of soil can influence nitrate leaching. For instance, clay soil, due to its low hydraulic conductivity, typically experiences less nitrate leaching compared to sandy soil. Therefore, soil testing, particularly in clay soils, can assist in optimizing nitrogen fertilizer recommendations and reducing leaching losses [36].

In conclusion, nitrogen loss from soils via various mechanisms has far-reaching implications on the environment and human health. Hence, a comprehensive understanding of these processes and the development of efficient strategies for nitrogen management are critical in promoting sustainable agriculture and protecting our environment.

2.7 Strategies to improve NUE

This section presents an array of strategies, ranging from tailored site-specific management to the integration of cutting-edge technologies, all aimed at bolstering NUE. Each subsection delves deeper into particular methodologies, offering insights into their efficacy and broader significance.

2.7.1 SSM and its evolution into precision agriculture

Enhancing NUE fundamentally depends on recognizing and addressing the varied requirements of different agricultural landscapes. SSM, approach in agricultural practices is the first step toward implementing PA. SSM provides recommendations for variable rate application (VRA) of nitrogen fertilizers based on the needs within a field, VRA enhancing NUE while minimizing environmental degradation [2], [92].

Several studies illuminate the promise of SSM [18], [31], [71], [103]. [31] investigated the use of site-specific nitrogen fertilization techniques. They employed a mechanical sensor designed to estimate the biomass of cereal plants. This sensor's data was then used to guide the application of nitrogen fertilizer, tailoring it to the specific needs of different areas within a field. This system yielded a notable 10-12% reduction in calcium ammonium nitrate use, without compromising grain yield or quality. Meanwhile, [18] assessed the economic viability of variable rate nitrogen application in wheat. Although conventional treatments yielded the highest, the cost efficiency of VRT made it a profitable choice. [103] tackled the challenge of soil nitrogen variability by implementing a VRA system equipped with Crop Circle ACS-430 sensors. These sensors were used to assess the nitrogen needs of crops in real time, allowing for precise and variable application of nitrogen fertilizer across different parts of a field. This technology-enabled approach led to a significant reduction in the total amount of nitrogen fertilizer used, while still maintaining high NUE and not compromising crop yield. [71] amalgamated proximal sensing, weather forecasting, and crop modeling to refine nitrogen

application in durum wheat. Their integrative method diminished nitrogen consumption and yield variability compared to traditional treatments.

The evolution of SSM into precision agriculture integrates advanced technologies such as remote sensing, GIS, and soil conductivity mapping. These tools enhance the robustness of the approach by offering detailed insights into field variability, thereby optimizing agricultural operations [2], [14]. [124] explored the applications of remote sensing and UAVs (Unmanned Aerial Vehicles) for crop monitoring and management. They identified a significant enhancement in the ability to detect early stress in crops, enabling more efficient water and nutrient applications. Furthermore, [56] emphasized the role of GIS in site-specific soil property and yield mapping. Their work showcased that integrating GIS with other technologies such as yield monitors can assist farmers in understanding spatial yield variability. On the front of soil health, [1] discussed the potential of soil electrical conductivity as an indirect measure for soil properties. Their research suggested that farmers can use this measure to adjust their soil management practices, leading to better nutrient and moisture management.

These studies underscore the transformative potential of integrating technology into precision agriculture. By harnessing these advanced tools, farmers can make more informed decisions, enhancing the productivity and sustainability of their operations.

2.7.2 Innovative techniques: N-rich strips and ramp application

N-rich Strip method: aim Strip trials are designed to determine the collective nitrogen needs of a field. By comparing different nitrogen application rates across various strips within the same field, they offer a comprehensive evaluation of the field's overall nitrogen requirement [86].

[62] conducted a study that underscores the efficiency of optical sensors combined with N-rich strips in managing nitrogen for winter wheat. Their research demonstrated that this sensor-based approach resulted in grain yields comparable to conventional

methods. However, it notably excelled in achieving higher NUE and reduced environmental impact, highlighting its effectiveness in precise nitrogen management.

Ramp Application: This method involves creating a strip in the field where nitrogen is applied at varying levels. Specifically, a Ramp calibration strip is a pass in the field with different nitrogen rates, typically involving at least five different rates, each extending at least 40 feet long, applied in addition to the normal starter nitrogen application [104]. It allows farmers to observe the crop's response to these different nitrogen levels, which aids in determining the optimal nitrogen application rate for the entire field [28]. [110] investigated multiple techniques for determining the nitrogen status of crops, highlighting the significance of real-time assessment to optimize nitrogen application. This research included methods such as Chlorophyll Meter (CM), Dualex Instrument, and remote sensing techniques, demonstrating a range of tools for accurate nitrogen management. Among these methods, the potential of ramp application was also acknowledged as an effective approach for assessing nitrogen needs Jones et al. [52] delve into nitrogen management for wheat, emphasizing the role of ramp application to optimize grain protein without compromising yield. The research underscores the importance of adaptive nitrogen techniques in dryland farming, and promotes tools like the MSU Small Grains Nitrogen Economic Calculator and strategies such as flag-leaf nitrogen concentration assessment to inform fertilization choices.

The integration of methods like N-rich strips and Ramp application with modern precision agriculture techniques can further optimize nitrogen application, ensuring that crops receive the right amount of nutrients at the right time.

2.7.3 AI, remote sensing, and their potential in NUE

The integration of AI and remote sensing technologies into precision agriculture has proven to be a watershed moment in the realm of modern farming [82]. These innovative technologies hold remarkable potential for advancing NUE by harnessing machine

learning algorithms and high-resolution remote sensing data [4]. The integration of these technologies has resulted in a more precise and efficient approach to nitrogen management, significantly enhancing the accuracy of nitrogen application and overall farm productivity.

AI, with its intrinsic capacity to handle vast datasets and model complex interactions, has become a potent tool in the hands of agriculturalists [4]. Specifically, machine learning (ML), a subset of AI, has shown immense promise due to its ability to predict outcomes with high accuracy. Various machine learning algorithms, such as Support Vector Machines (SVM), Artificial Neural Networks (ANN), and Random Forests, have found utility in nitrogen management [50]. These innovative algorithms, through a learning process that relies on historical and current agricultural data, can predict crop yield, nutrient uptake, and optimize nitrogen application rates with considerable precision.

Further advancing the possibilities of ML in crop yield prediction, a study by [117] explored the application of five distinct machine learning algorithms, including linear regression (LR), decision tree (DT), SVM, ensemble learning (EL), and Gaussian process regression (GPR) in predicting the yield and dry matter of winter wheat in the North China Plain. The study found that the GPR model surpassed all other models in accuracy, with the prediction errors for maximum yield and dry matter being only 5.8% and 1.1%, respectively. This study gives credence to the idea that AI and ML can provide more precise predictions, informing the optimal application of water and nitrogen to achieve maximum yield and dry matter, thereby increasing NUE.

Research has been conducted to examine how different soil properties, such as water-holding capacity and organic matter content, affect NUE within smaller, specific areas of a field. These studies aim to understand NUE's variability at a more localized or subfield level. [46] quantified NUE in dryland winter-wheat fields in Montana following several years of variation in experimental N fertilizer applications. Through a comparison

of six candidate models, they developed a model capable of predicting NUE at a subfield scale. The results of their study showed that a random forest regression model provided the least error in predicting NUE. Thus, their work highlights the potential of AI in enhancing our understanding of soil dynamics and optimizing nitrogen fertilizer use, thereby improving NUE.

Lastly, a compelling demonstration of the synergistic potential of AI and remote sensing technologies can be seen in the work of [58]. This study combined the use of UAV-based Vegetation Indices (VIs) and ML models to predict corn field yield at different growth stages. Notably, the study revealed that support vector regression (SVR) and k-Nearest Neighbor (KNN) models outperformed other ML models in yield prediction. Importantly, this study showed that these technologies could make accurate yield predictions, even with a limited number of training data, reinforcing the scalability and robustness of these AI and remote sensing-based approaches.

The convergence of AI and remote sensing technologies, as seen in these studies, offers promising ways to advance NUE, underscoring the potential of these technologies in optimizing nitrogen management and bolstering sustainable agricultural practices.

2.7.4 Applied nitrogen management in wheat and corn

Considering the global importance of wheat and corn, targeted nitrogen management strategies for these crop hold special significance [114]. Integrating techniques from SSM, precision agriculture, and AI can significantly enhance NUE in the cultivation of these staples [2], [10], [114].

In wheat cultivation, a comprehensive study [50] was undertaken to develop an efficient nitrogen management strategy based on multi-source data. The researchers collected data from UAV multi-spectral images, plant sampling, weather, and field management to establish and validate the strategy. Machine learning methods, particularly the Random Forest algorithm, were utilized to integrate the multi-variate information to

determine the optimal parameters in the nitrogen regulation algorithm. This innovative strategy enhanced energy use efficiency and net profit while decreasing nitrogen input, energy input, and CO_2 emissions, all without any reduction in yield.

Another unique approach [116] was developed which combined crop growth modeling, active canopy sensing, and machine learning for an in-season nitrogen management strategy in corn production. The strategy enabled accurate prediction of the in-season economic optimal side-dress nitrogen rate (EOSN). The recommended EOSN demonstrated a high correlation with measured values, thus showing the promising potential of the combination of crop growth modeling, active canopy sensing, and machine learning for in-season site-specific nitrogen management.

Furthermore, a detailed study [6] focused on understanding the relationship between data derived from an unmanned aerial vehicle (UAV) platform and the crop's temporal and spatial variability in small wheat fields. The variable rate nitrogen application strategy implemented in this study led to an overall decrease in nitrogen fertilizer application between 5 and 40%, depending on the field heterogeneity. In the majority of case studies, NUE was improved by approximately 10% by redistributing and reducing the amount of nitrogen fertilizer applied.

These studies underline the effectiveness and promising potential of integrating sensor-based precision agriculture techniques and machine-learning algorithms into nitrogen management strategies for wheat and corn.

2.8 Research gap

Research on NUE has been extensively conducted, yet several unexplored avenues remain. Addressing these gaps is imperative, especially for crucial crops such as wheat and corn, as this can promote sustainable and efficient agricultural practices.

1. **Broadening the Scope:** Many current studies are predominantly confined to precision agriculture and NUE for specific crops and locations [37]. To maximize

the benefits of precision agriculture techniques, there is a need to expand research to a wider range of agricultural settings.

2. **AI Integration:** Though there is an increasing interest in integrating AI into nitrogen management, its full potential remains underutilized. A large number of studies use generic AI models without tailoring them to address the specific challenges of agriculture [54]. There is a clear demand for AI models that are fine-tuned to the nuances of nitrogen management.

3. **Real-time Monitoring with Image Processing:** Traditional agricultural practices often rely on data sources like soil sensors and past yield data, which can be influenced by unpredictable factors [81]. AI-driven image processing can offer continuous, real-time monitoring and analysis of crop conditions, enhancing the accuracy of nitrogen needs assessment.

4. **Advanced Image Processing:** Many image processing techniques in agriculture still employ basic methods or automated software like Pix4d. The limitations, such as stitching inaccuracies, necessitate a shift towards advanced, AI-based image processing techniques that offer in-depth analysis.

5. **AI and Remote Sensing Synergy:** The integration of AI with remote sensing tools, including drones and satellites, remains a largely unexplored area. This combination can offer comprehensive insights into crop nitrogen needs, optimizing management practices.

2.9 Research objectives

In response to the above-mentioned research gaps, this study aims to deepen our understanding of NUE practices, particularly for wheat and corn. The research objectives were:

1. To evaluate the crop response to nitrogen application by implementing N-rich reference spots within different management zones in a field.

2. To improve the NUE in wheat and corn production.

3. To design and implement an AI-based image processing techniques to analysis remote sensing data.

4. To develop an approach that integrates AI-derived imagery analysis with historical field data to generate N prescription map.

3 Methodology

3.1 Overview of the methodology

18.23.2 This chapter outlines the research methodology for wheat and corn NUE strategies in South Dakota. Detailed information about the experimental sites is provided in Section 1.9. We have employed a multi-faceted approach, combining precision agriculture practices with AI and remote sensing technologies, to examine and optimize nitrogen application. A simplified overview of the research methodology is illustrated in Figure 3.1.

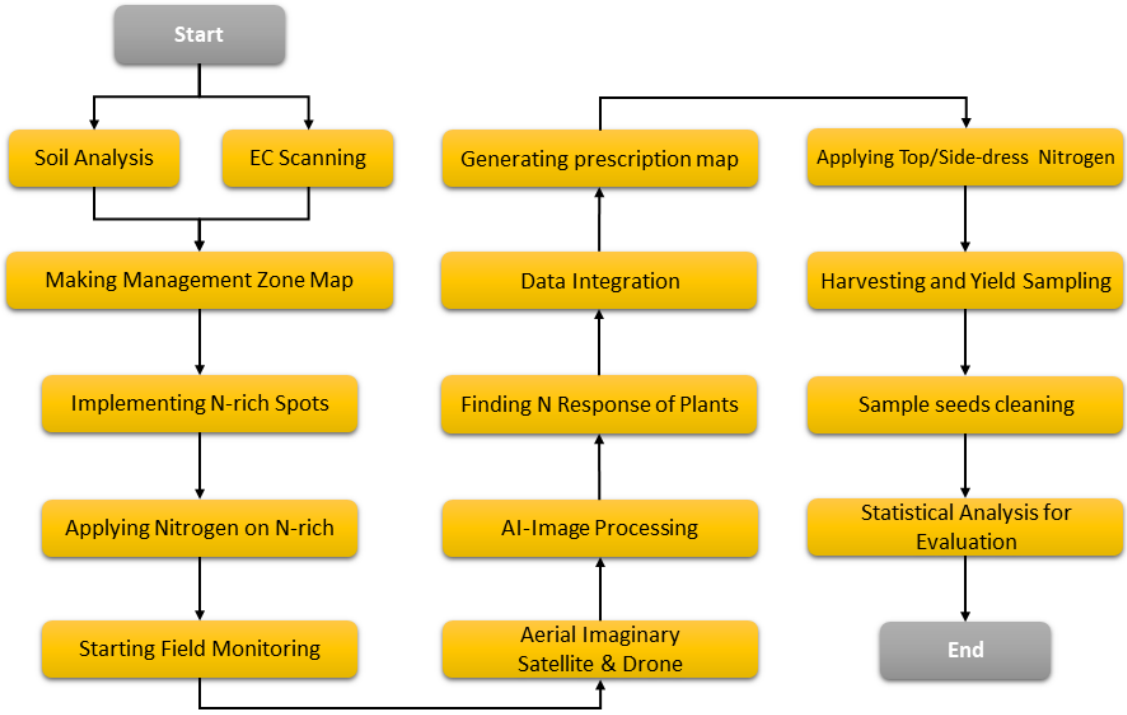

Figure 3.1: An overview of the research methodology employed in optimizing NUE for wheat and corn cultivation.

This visual representation provides a snapshot of the stages and processes undertaken, from initial field scanning and planting to the analysis of aerial and satellite images, and eventually to analyzing the harvesting data. The following sections will offer exploration of each component of the methodology, techniques, materials, and analyses

that strengthen outcomes of this study.

3.2 Creating management zones

In this research, we start with creating management zones to categorize different areas of a field based on their potential productivity. Creating these management zones is crucial as it allows for tailored agronomic practices that match the specific needs of each zone, optimizing inputs like fertilizers for enhanced efficiency and yield. To achieve this, Soil Electrical Conductivity (EC) Scanning is employed, followed by soil analysis. These methods complement each other for defining management zones, which optimize agricultural practices.

3.2.1 Soil EC scanning

To begin with, we utilized Soil EC scanning as a method to create management zones for precision farming. For this purpose, we used the EM38-MK2 Ground Conductivity Meter to conduct the scanning. This efficient and non-invasive technique measures the soil's ability to conduct electrical current, thereby revealing the spatial variability of soil properties. Through EC scanning, we identified variations in soil conditions that informed the creation of tailored management zones to address these specific conditions.

Zone maps, generated from EC scanning data, served as visual guides for soil property distribution across the field. These maps were instrumental in guiding localized management decisions and ensuring representative sampling for further detailed analysis.

Before we began the scanning, it was essential to calibrate the EC scanner device to ensure accurate and reliable data collection. The calibration of EC machines is a pivotal step that involves contrasting the machine's readings with a known standard and requires ongoing attention to ensure the accuracy of the measurements. The calibration process, as delineated in the device's manual, is summarized as follows:

Calibration procedure for the EM38-MK2 Ground Conductivity Meter

1. Initial Setup:
    - Situate the EM38-MK2 in the air, ensuring its operation in the horizontal dipole mode.
    - Neutralize the Q/P readings to zero to ascertain a standardized starting point.
2. Adjusting the Q/P Zero Control:
    - Preset the Q/P zero control to a predetermined arbitrary value, for instance, H=10 mS/m, as a foundational reference.
    - Transition the instrument to the vertical dipole mode.
    - Record the indicated reading, which might hypothetically be V=16 mS/m.
    - Derive the difference between the vertical and horizontal readings, e.g., $V - H = 6$ mS/m in the provided hypothetical scenario.
3. Final Adjustments:
    - While in the horizontal dipole mode, modify the Q/P zero control until the display showcases a value double of that deduced in the prior step, making it 12 mS/m in our illustrative example.
4. Validation:
    - Elevate the instrument to a minimum of 1.5 meters from the ground. The resulting Q/P reading or conductivity must invariably align with the equation: $V = 2H$.
5. Coil Separation Setting (if required):
    - If utilizing a 0.5 m coil separation, adjust the MODE to the corresponding 0.5 m setting.
    - Redo steps 1 through 3 under this configuration.

- Notably, when the 0.5 m setting is active, procedures demanding a 1.5 m elevation can be substituted by a mere 0.75 m height.

Figure 3.2 shows a researcher calibrating the device. Regular recalibrations, as outlined, are essential for optimal performance and accurate assessments of soil properties. Before each scanning session, we performed a calibration to ensure the reliability of the data collected. After calibration, we initiated the scanning process, covering a swath of 10 meters (approximately 32.8 feet) in each pass across the field.

Figure 3.2: A researcher calibrating the EM38-MK2 Ground Conductivity Meter.

Upon completing the scanning process, we utilized SMS software to create management zones based on the data gathered. In our methodology, we delineated five distinct zones. Subsequent to the creation of these zones, we conducted soil sampling to gather supporting data that further validated and enriched our understanding of the

established zones.

3.2.2 Soil sampling and analysis

Soil sampling refines the broader overview offered by EC scanning, working in synergy to yield a thorough comprehension of soil attributes and further enhancing the credibility of zone maps.

Our soil sampling strategy, guided by standard protocols for agricultural soil analysis, incorporated directed sampling based on EC data [23]. This approach allowed us to target specific areas within the field that exhibited varying EC levels, ensuring a more precise and representative analysis of soil characteristics.

- Sampling was conducted at 0-12 inches depth, and multiple samples from the same spot were combined to form a composite sample, ensuring a holistic representation of that location
- A soil auger, facilitating the collection of soil samples from specific depths, as shown in Figure 3.3, ensuring accurate analysis of varying soil properties at different layers

Figure 3.3: Soil Sampling Process. On the left, a researcher is shown in the field, actively using the auger for soil sampling. On the right, a soil auger is depicted with a freshly extracted soil sample.

After collection, soil samples were analyzed and essential features for our research were extracted and quantified.

In our methodology, we synthesized EC data and soil sampling results to craft precise management zones. This process entailed aligning EC readings with soil texture and fertility data obtained from various depths to define distinct zones based on soil characteristics.

3.3 Establishing N-rich spots

The N-rich spots are designed as circular areas with a diameter of 18 meters (approximately 59 feet), ensuring they are small enough to use less nitrogen in the test phase and big enough to be discernible in satellite imagery. In this methodology, three spots are established within each zone with a tile positioned at the center of every spot. These tiles serve as markers for identifying spot centers in aerial images and as reference points for bio-sensing nitrogen application. These spots serve as biological (bio) sensors, gauging plant responses to nitrogen application across different areas. This approach offers several advantages over methods such as the N-rich strip, which involves applying nitrogen to large strips across the field. The small size of these spots allows for their repeated placement within a zone, ensuring a comprehensive understanding of the entire area. Additionally, the minimal nitrogen required for these spots makes this approach cost-effective. The adaptability in positioning circular spots proves advantageous, especially in fields with irregular zones. Figure 3.4 illustrates N-rich spots on a field with tiles positioned at their centers.

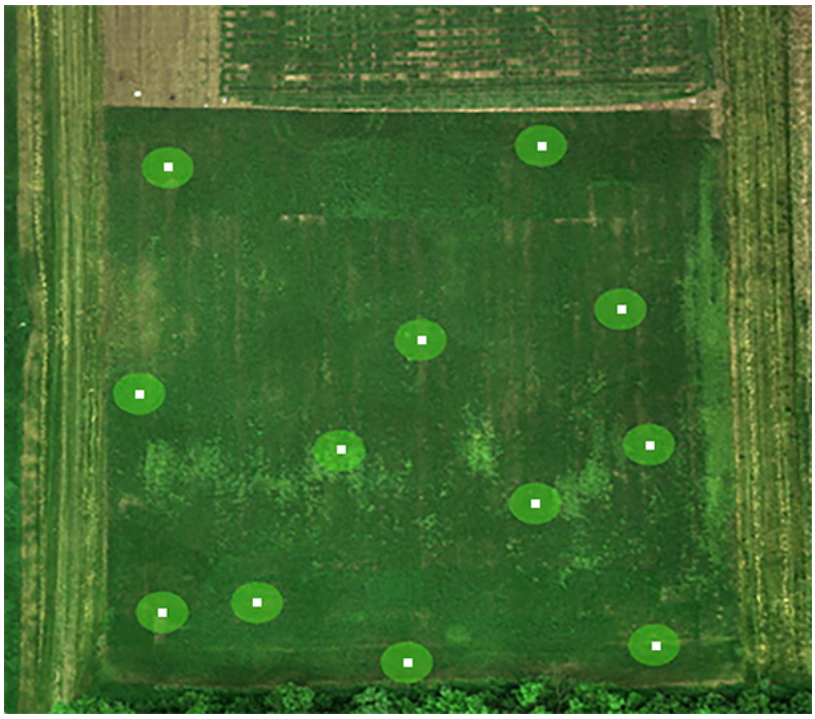

Figure 3.4: Schematic representation of the field showing N-rich spots with tiles positioned at their centers.

After establishing N-rich spots, nitrogen is applied across all designated spots using a manual fertilizer spreader, a compact, two-wheeled device pushed across the field, as shown in Figure 3.5. For each application, 27 pounds of urea, containing 46% nitrogen, are used per spot. This equates to 11.5 lbs. of nitrogen per spot, translating to an application rate of approximately 397.46 lbs. of urea or 182.8 lbs. of nitrogen per acre.

Figure 3.5: Nitrogen Application Process. The image showcases a researcher using a manual fertilizer spreader to apply nitrogen to one of the N-rich test spots.

3.4 Field monitoring

After establishing the N-rich spots, continuous field monitoring was initiated and maintained until the end of the harvesting period to ensure the integrity of the experiment. Regular checks were conducted to identify growth inconsistencies, prevent diseases, and validate data using tools such as the GreenSeeker device and tape measures. These measures ensured that observed differences in growth or yield were attributed to experimental variables, thereby enhancing the reliability and validity of our findings.

Figure 3.6: Measuring the height of wheat plants in different zones using a tape measure.

3.5 Drone-based multi-spectral imaging

After applying nitrogen to the designated spots, we transition to the next phase of our methodology: capturing aerial images to analyze the plants' response to the nitrogen application. Drone imagery is integral to our approach, facilitating the collection and analysis of field data. This stage is timed to coincide closely with the top-dress period of

wheat, which is typically between 400 to 600 growing degree days [112], allowing for an optimal assessment of the plants' nitrogen uptake efficiency. For the corn field, being a dedicated plot provided by a local farmer, the decision regarding the optimal timing for side-dressing was determined by the farmer based on their time window.

We utilized a drone (DJI Phantom 4 pro) equipped with a multi-spectral camera, featuring a 12-megapixel lens with a focal length of 5.4 mm and an aperture value of F1.5. The camera is capable of capturing images in five distinct bands: Red, Green, Blue (RGB), Red Edge, and Near-Infrared (NIR). These bands were selected for their ability to provide valuable insights into plant health and soil properties.

To initiate the process, we prepared a Keyhole Markup Language (KML) file outlining the precise boundaries of the field of interest. This file was uploaded to the drone's flight control software, guiding the drone to follow a flight path over the field. This ensured coverage of the area while minimizing overlaps. The drone flew at an altitude of 200 feet (60.96 meters) over the wheat field and 400 feet (121.92 meters) over the corn field.

The resulting imagery comprised two separate files, each with a resolution of 4000 x 3000 pixels, capturing the aforementioned five bands.

3.5.1 Image calibration

Aerial images can display variations in brightness and other visual attributes due to various external factors such as time of capture, cloud coverage, shadows, and more. Such inconsistencies, if not addressed, can introduce errors in subsequent analyses, especially when comparing images from different times or conditions.

To address this challenge, we employ a calibration procedure using a reflectance panel. The primary function of this calibration panel is to provide a consistent reference point across all captured images. As the drone flies over the field, it also captures images of the calibration panel. Figure 3.7 displays a drone flying over our calibration panel,

which is vital for this calibration process.

Figure 3.7: A drone, equipped with a multispectral camera, captures imagery over a calibration panel, ensuring precision in data on the image acquisition day.

Our chosen calibration panel, provided by Sentera, has specific reflectance values for each band, as detailed in Table 3.1.

Table 3.1: Reflectance values of the Sentera calibration panel for different bands. The values, ranging between 0 and 1, represent the fraction of light reflected by the panel relative to the incoming light.

Bands:	Blue	Green	Red	Red-Edge	NIR
Reflectance:	0.1059	0.1054	0.1052	0.1052	0.1055

3.5.2 Calibration procedure

Image calibration is a cornerstone in ensuring data consistency and eliminating possible deviations due to external factors. Leveraging Python for this task allows for an

automated, efficient, and reproducible calibration process. Here's a step-by-step breakdown of how we've approached this crucial stage using Python:

Load Images: Import captured images into a Python environment using PIL library. Convert images to a 16-bit format if they are in 8-bit, ensuring a higher precision during the processing phase.

Preprocess Images: Apply a Gaussian blur to diminish high-frequency noise, aiding in more robust calibration panel detection. Resize and normalize images to ensure a uniform scale and intensity distribution, which aids in consistent processing across different images.

Identify Calibration Panel: Utilize advanced object detection models for precise detection of the calibration panel within the images. Specifically, the model based on the Faster R-CNN architecture, as detailed in section (3.7), is employed for this purpose. Validate detected regions using shape analysis, confirming the calibration panel's presence based on its characteristic form.

Extract Reflectance Values: Define the Region of Interest (ROI) from the detected calibration panel to measure reflectance values for each band. Use spectral unmixing techniques to derive pure reflectance values, particularly beneficial in overlapping spectral regions.

Radiometric Calibration: Compute a calibration factor by comparing the reflectance values obtained from the images to the standardized values from the Sentera calibration panel. Apply this factor across all pixels in the bands to achieve radiometric calibration of the images.

Atmospheric Correction: Implement the Dark Object Subtraction method to further refine the reflectance values by accounting for atmospheric interferences, ensuring the images' accuracy.

Adjustment: Normalize image histograms for maintaining consistent brightness and contrast across all images, especially if captured under varying conditions. If multiple

images are being analyzed, ensure their alignment using image registration techniques, which guarantees accurate comparisons.

Save Calibrated Images: Opt for lossless formats like TIFF when saving images to retain the integrity and precision of the calibrated data. Accompany the images with metadata, encapsulating calibration factors, parameters, and other pertinent information for future references.

This calibration process ensures that our aerial images are consistent and accurate, allowing for a reliable comparison and subsequent analyses. Using standardized reflectance values and adjusting the images accordingly guarantees that the information derived from them is dependable and actionable for our study's objectives.

3.6 Satellite imagery

To ensure the continuity and robustness of our study, we complement our drone-based image collection with satellite imagery from the Sentinel satellite, part of the European Space Agency's Copernicus Programme. The Sentinel satellite provides high-resolution, multi-spectral imagery that enhances our understanding of field conditions over time, offering a broader perspective and complementing the detailed insights from our drone-based images. This approach acts as a contingency plan, offering backup data for our analysis when drone flights are hindered by unfavorable weather conditions, unavailability of the drone, or inaccessible fields. It also enables us to compare analyses based on both satellite and drone data. We chose the Sentinel-2 satellite for its superior spatial resolution of up to 10 meters, cost-free data access, and extensive geographical coverage, which ensures detailed analysis and consistent data collection. Additionally, the Sentinel-2 satellites offer a revisit frequency of 10 days for each individual satellite, but with the combined constellation, this interval is reduced to 5 days. This frequent revisit capability allows for more timely and accurate monitoring, making it highly suitable for our study's needs.

3.7 Faster R-CNN model

The prevalent methods for analyzing aerial photos in agriculture involve merging numerous images into one cohesive image using software such as Pix4D, followed by computing the NDVI or other spectral indices using the same or similar software. While this approach has its advantages, it also harbors certain drawbacks. Merging images can lead to a loss of resolution, as the process essentially averages the information from multiple photos, reducing the detail visible in the final image. Moreover, areas where images overlap can cause shadowing effects or misinterpretations of the spectral information, skewing the resulting analysis. These challenges can limit the precision and effectiveness of traditional image analysis.

To circumvent these challenges, we propose a novel approach that leverages the power of deep learning. By forgoing the merging of images, we retain the original image quality and avoid the issues associated with overlapping areas. Specifically, we employ the Faster R-CNN model [88], a state-of-the-art object detection algorithm that offers key benefits for our task. This model is adept at detecting and localizing tiles within the high-resolution, individual aerial images of the field, negating the need for image merging. Considering we potentially have hundreds of images to process, the efficiency of the Faster R-CNN in handling large datasets, along with its high accuracy in object detection and localization, makes it an ideal tool for our approach. By preserving the original image quality and leveraging precise object detection, our methodology aims to enable a more accurate and reliable analysis of field conditions and crop health. The structure of Faster R-CNN is illustrated in Figure 3.8.

Faster R-CNN features a two-part design. The first part is the RPN that scans the image and generates potential bounding boxes that could contain an object. The second part is a Fast R-CNN network that takes these proposed regions and classifies them, determining what object, if any, they contain.

This two-step process offers several advantages. Firstly, it allows for high

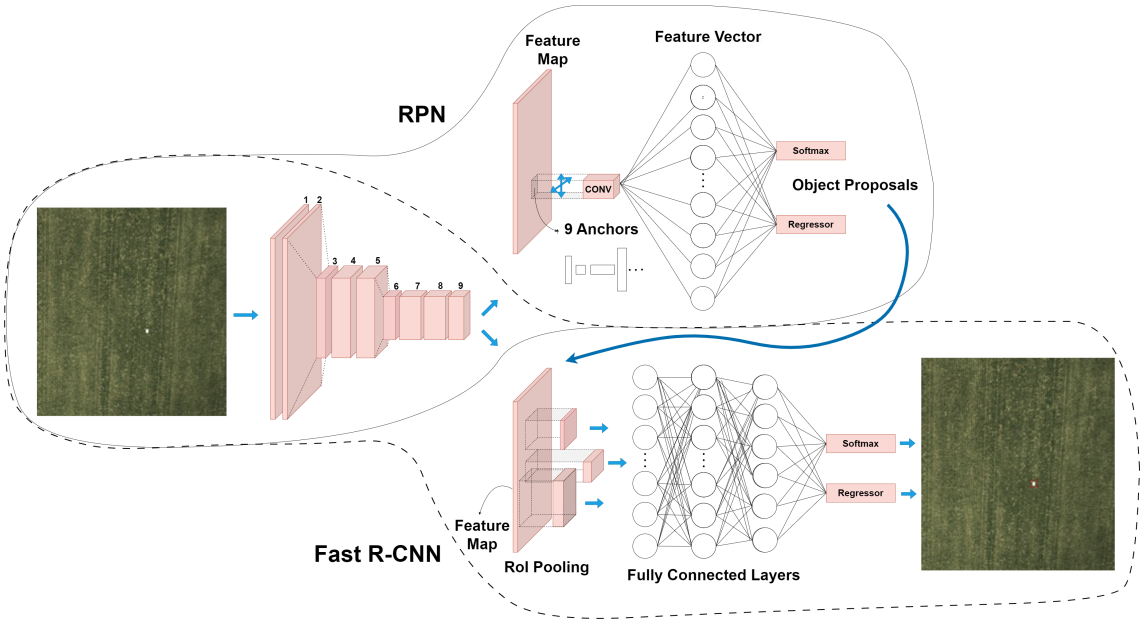

Figure 3.8: Schematic representation of the Faster R-CNN architecture, showing the Region Proposal Network (RPN) for candidate regions and the Fast R-CNN for object classification and bounding box refinement.

precision in detecting objects as the network can learn to propose regions that are likely to contain objects of interest and ignore irrelevant areas. This not only improves accuracy but also increases speed as fewer regions need to be processed. Secondly, the use of convolutional layers enables the model to handle input images of any size and aspect ratio, a flexibility that is highly desirable in practical applications. Lastly, because the network is fully differentiable, it can be trained end-to-end with backpropagation, which simplifies the training process and often results in better performance.

For our task, the Faster R-CNN model offers some key benefits. It can efficiently detect and localize the tiles and calibration panel in the aerial images of the field. Given that we have potentially hundreds of images to process, the efficiency of Faster R-CNN in handling large datasets is highly beneficial. Moreover, its accuracy in detecting and localizing objects will enable us to precisely identify the tiles and measure their size in the image, which is crucial for our analysis.

3.7.1 Training process

Training the Faster R-CNN for our specific task involves the following steps:

Image Annotation: First, we need to manually annotate a subset of our images by identifying both tiles and calibration panels. This involves drawing bounding boxes around each object and assigning it the appropriate class label, either as a 'tile' or a 'calibration panel'. These annotated images serve as the ground truth.

Model Training: We used a total of 500 labeled images for training without employing any data augmentation techniques. These images were fed into the Faster R-CNN model without using any pre-trained weights. The model was configured with a batch size of 4, optimizing the learning process for our dataset size. An adaptive learning rate strategy was employed, starting at 0.001 and gradually increasing to adapt to the model's learning progress. This approach enhanced the training effectiveness, especially given the limited size of our dataset. The training was conducted over 100 epochs, ensuring comprehensive learning and adaptation by the model. During training, the model learned to recognize tiles and calibration panels based on their visual features, proposing regions likely to contain these objects (using the Region Proposal Network, RPN) and classifying these regions (using the Fast R-CNN).

Model Evaluation: During the training process, we periodically evaluated the model's performance on a validation set of 100 images that it had not seen before.

Model Testing: Once training was finalized, we conducted a rigorous test using a distinct set of 100 images.

Model Deployment: Finally, we deploy the trained model to detect and localize tiles in the remaining images. The model's outputs, including the bounding boxes and class predictions, are used in further analysis.

In conclusion, the Faster R-CNN model, with its ability to efficiently and accurately detect and localize objects in images, provides a robust solution for our task. By training the model on our specific task, we can fine-tune its capabilities to our specific

needs, ensuring high performance in detecting the tiles in the aerial images.

3.8 Converting image measurements to real-world dimensions

Following the identification of tiles within drone-captured images by the Faster R-CNN model, our methodology proceeds with calculating the size of these detected tiles and assessing the coverage of the spot. These steps are critical in quantifying the effectiveness of nitrogen application. The detailed procedures are as follows.

3.8.1 Calculation of tile dimensions in images

The primary step in this process entails determining the size of the tile as detected within the image. This calculation leverages the dimensions of the bounding box—namely, its height and width—delivered by the Faster R-CNN model. The pixel area of the tile within the image, represented as $A_{\text{tile\_pixel}}$, can be quantified through equation 3.1.

$$A_{\text{tile\_pixel}} = \text{width}_{\text{bbox}} \times \text{height}_{\text{bbox}} \tag{3.1}$$

Here, $\text{width}_{\text{bbox}}$ and $\text{height}_{\text{bbox}}$ correspond to the bounding box's width and height, respectively.

However, this computed pixel area does not directly mirror the real-world dimensions of the tile. To bridge this gap, we employ a conversion process using known physical dimensions of the tiles, which are 12 inches by 12 inches (or equivalently, 30.48 cm by 30.48 cm).

The image scale plays a pivotal role in this conversion. It is affected by the drone's altitude and camera specifications. Our drone flights were conducted at altitudes of 200 feet (60.96 meters) over wheat fields and 400 feet (121.92 meters) over corn fields. The camera specifications, including a 12-megapixel lens with a focal length of 5.4 mm, an aperture value of F1.5, and sensor size of 1/2.9" CMOS, also influence the image scale. This scale, defined as the ratio of a distance on the ground to its representation in the

image (in pixels), is crucial for converting pixel measurements to real-world dimensions.

To calculate this scale, we first determined the camera's horizontal Field of View (FoV), which was found to be approximately $60.43°$, based on the focal length and sensor size as shown in Equation 3.2. Then, we calculated the Ground Sample Distance (GSD) – the distance between the centers of two consecutive pixels as represented on the ground. At 200 feet, the GSD was approximately 0.01775 meters per pixel, and at 400 feet, it was about 0.0355 meters per pixel. Consequently, the scale factor – representing how many meters in the real world are depicted by each pixel in the image – was calculated as approximately 17.17 meters per pixel at 200 feet and 8.59 meters per pixel at 400 feet. These scale factors were then used to accurately convert the tile dimensions from the pixel measurements in the images to their real-world sizes, ensuring precise and reliable data for our analysis.

$$\text{FoV } = 2 \times \arctan\left(\frac{\text{sensor width}}{2 \times \text{ focal length}}\right) \tag{3.2}$$

With the known scale, we can calculate the real-world area of the tile, denoted as $A_{\text{tile\_real}}$, using equation 3.3.

$$A_{\text{tile\_real}} = \frac{A_{\text{tile\_pixel}}}{\text{scale}} \tag{3.3}$$

In this equation, 'scale' acts as the conversion factor that translates pixel-based measurements into real-world dimensions.

In a case where the scale is not directly known, it can be determined using the known physical dimensions of the tile and its size in the image, represented as $A_{\text{tile\_physical}}$ and $A_{\text{tile\_pixel}}$, respectively. The scale can then be expressed as equation 3.4.

$$\text{scale} = \frac{A_{\text{tile\_physical}}}{A_{\text{tile\_pixel}}} \tag{3.4}$$

This calculated scale is consistently applicable across images taken at the same

altitude and with identical camera settings, facilitating reliable conversion of tile sizes for various images.

Through these calculations, we effectively translate the tile dimensions detected in images into real-world dimensions, laying a solid foundation for accurate determination of spot coverage.

3.8.2 Assessment of spot coverage

Upon successfully converting the tile size from the image to its real-world dimensions, we advance to the critical process of determining the spot coverage. This stage involves contrasting the real-world size of the identified tile, represented as $A_{\text{tile\_real}}$, with the predetermined size of the spot, denoted as A_{spot}. A_{spot} is gleaned from the field layout and is an important parameter for the task at hand.

Given the circular nature of the spots, the spot's area can be computed using the known diameter size (D_{spot}) input from the field layout. We set the radius of each spot at a minimum of 8 meters to ensure full visibility in the satellite images. This is due to the resolution of the Sentinel satellite images, where a single pixel can cover approximately 10x10 meters on the ground, or sometimes, this may vary depending on the satellite's altitude. Hence, by setting the radius at 8 meters or more, we can ensure that each spot occupies at least one full pixel in the satellite image. Utilizing the formula for the area of a circle, we can calculate the spot's real-world area as equation 3.5.

$$A_{\text{spot\_real}} = \pi \left(\frac{D_{\text{spot}}}{2} \right)^2 \tag{3.5}$$

Here, π approximates to 3.14159, and $\frac{D_{\text{spot}}}{2}$ gives the radius of the circular spot.

The comparison of $A_{\text{tile\_real}}$ and $A_{\text{spot\_real}}$ is not to equate them but rather to assess the position of the tile within the spot. The tile, placed in the center of the spot, acts as a marker for the spot center in the images captured. If $A_{\text{tile\_real}}$ is smaller than $A_{\text{spot\_real}}$ and is centrally located in the image, it implies that the entire spot is within the frame of the

image. Mathematically, this coverage condition can be represented as:

$$\text{if } A_{\text{tile\_real}} < A_{\text{spot\_real}} \text{ and tile is centrally located: image is deemed acceptable}$$

The determination of whether the tile is centrally located can be done using the bounding box's position information provided by the Faster R-CNN model.

The comprehensive nature of this methodology, involving both tile size measurement and spot coverage determination, underpins the robustness of the ensuing phases of the analysis. By ensuring only images truly representative of entire spots are selected, the reliability and validity of the nitrogen application effectiveness evaluation are significantly enhanced.

This meticulous approach, therefore, underpins the reliability of the overall study, ensuring accurate and trustworthy results in the quest for sustainable and effective nitrogen application practices.

3.9 Nitrogen response analysis using image processing

Understanding plant responses to nitrogen application is pivotal for optimizing its use in farming. In the preceding section, we utilized object detection models to identify best candidate for each spots in the field. Now, with the most representative image for each spot identified, our focus shifts to discerning the differences between areas where nitrogen was applied and areas where it was not. The ultimate goal is to determine zones where nitrogen application spurred growth, indicating that nitrogen was previously a limiting factor, and zones where growth remained stunted post-application, implying the limitation stemmed from factors other than nitrogen. As we delve deeper, image normalization becomes an indispensable step, letting us tap into the rich insights various normalized images present.

3.9.1 Utility of NDVI

The NDVI is a fundamental tool in remote sensing used to gauge the density and health of live green vegetation in an image. Representing a dimensionless index, NDVI values oscillate between -1 and 1, with values nearing 1 indicating healthier vegetation.

Derived from the near-infrared (NIR) and red bands of an image, the NDVI is calculated as equation 3.6.

$$\text{NDVI} = \frac{\text{NIR} - \text{Red}}{\text{NIR} + \text{Red}} \tag{3.6}$$

Here, NIR denotes the near-infrared band value, while Red signifies the red band value. The preference for these bands stems from their correlation with plant health. Healthy plants with abundant chlorophyll absorb more red light for photosynthesis, while their cell structure reflects near-infrared light. Consequently, image areas exhibiting healthy vegetation usually showcase higher NDVI values.

Leveraging normalized indices like NDVI offers distinct advantages. NDVI, in comparison to singular spectral bands, exhibits reduced sensitivity to alterations in atmospheric factors and illumination conditions. Additionally, it furnishes a more direct metric of vegetation health and vigor.

3.9.2 Utility of Excess Green Index (ExG)

ExG or Excess Green Index is another significant measure in remote sensing employed to identify vegetation within images. The ExG, as the name suggests, emphasizes the greenness of an image, providing a clear distinction between vegetation and non-vegetation areas. It is a straightforward and effective method for segmenting plants in digital images.

The ExG Index is calculated as Equation 3.7.

$$\text{ExG} = 2 \times \text{Green} - \text{Red} - \text{Blue} \tag{3.7}$$

Where Green, Red, and Blue represent the respective color channels of an image.

ExG is particularly beneficial when analyzing areas with dense vegetation. In combination with NDVI, it provides a comprehensive understanding of vegetation health, density, and overall vigor.

3.9.3 In-spot vs. Out-spot analysis

After determining the NDVI and ExG values for each spot, we proceed to sample specific areas from both in-spot (where nitrogen was applied) and out-spot (without nitrogen application) for a comparative analysis of their NDVI and ExG distributions. The primary objective of this comparison is to ascertain the extent of plant response to the applied nitrogen in the designated areas.

As depicted in Figure 3.9, the in-spot area is identified and a sample consisting of 250x250 pixels is extracted. To ensure accuracy in our calculations, any tile present within the sampled area (used to indicate the center of the spot) is replaced by the average pixel values from the surrounding in-spot area. This ensures the tile does not influence subsequent calculations.

Additionally, four distinct samples, each of the same size as the in-spot, are taken from the out-spot where no nitrogen was applied. An average image is constructed from these four samples, creating a single representative image. Both the in-spot and averaged out-spot images are then processed by the Wasserstein algorithm to evaluate the extent of their differences.

To verify the uniformity of the out-spot samples, which serve as our controls for the in-spot center, we selected three separate locations within the zone. By comparing their standard deviations to the average of the original four out-spot samples, we assess consistency across the zone. If the variance is minimal (a standard deviation close to

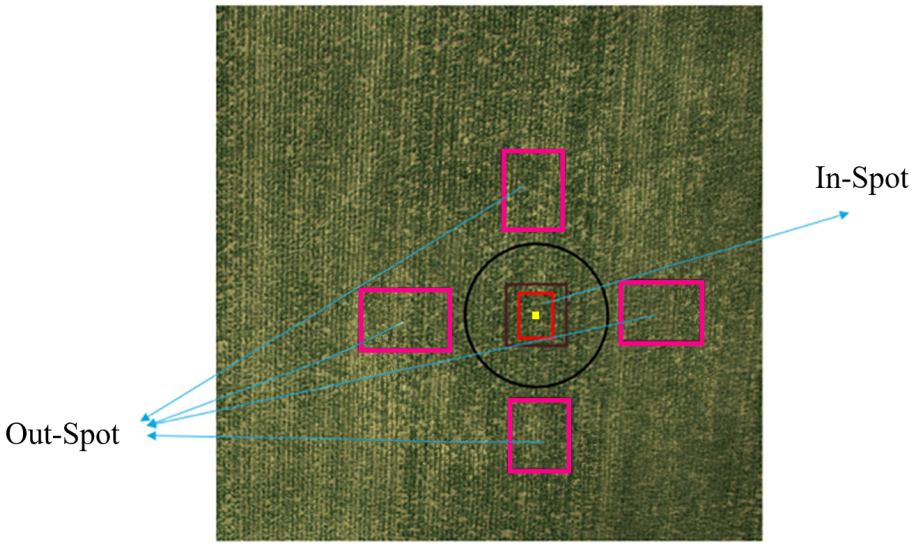

Figure 3.9: Visual representation highlighting the central 'in-spot' where N was applied, juxtaposed with four 'out-spot' regions, the areas without N application.

zero), this indicates that the forthcoming comparison is unbiased and unaffected by potential variations in the zone. Figure 3.10 conceptually illustrates this comparison across different parts of a given zone.

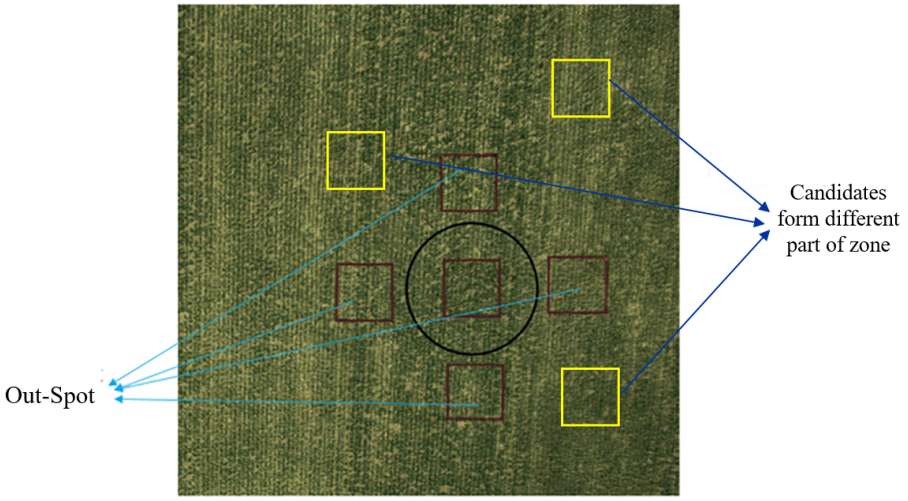

Figure 3.10: Schematic representation highlighting the three sampled locations within a nitrogen-deprived zone, juxtaposed against the four control spots.

3.9.3.1 Wasserstein distance

To draw a quantitative comparison between the in-spot and out-spot distributions, the Wasserstein distance is employed. Also dubbed as the Earth Mover's Distance, this measure metaphorically denotes the 'work' required to morph one distribution into another.

The Wasserstein distance can be conceptually imagined as the effort necessary to shape one distribution pattern into another, as demonstrated in Figure 3.11.

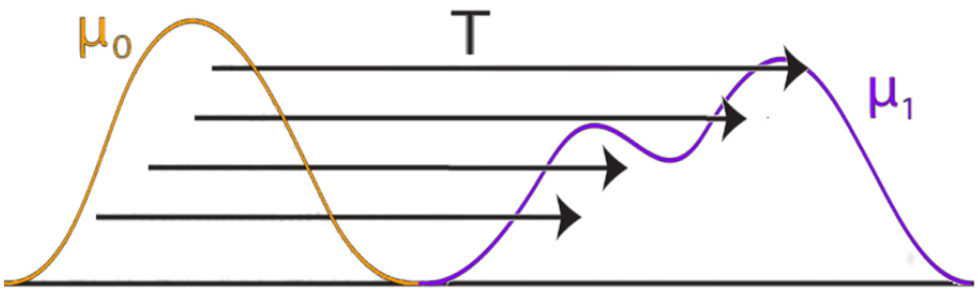

Figure 3.11: Visualization of the Wasserstein distance between two distributions, illustrating the shift needed to transform one distribution into the other one

For two probability distributions P_{in} and P_{out} epitomizing the in-spot and out-spot NDVI or ExG distributions, the Wasserstein distance $W(P_{\text{in}}, P_{\text{out}})$ can be ascertained as equation 3.8.

$$W(P_{\text{in}}, P_{\text{out}}) = \inf \int |x - y| \, d\pi(x, y) \tag{3.8}$$

Here, inf stands for the infimum over all joint distributions $\pi(x, y)$ with marginals P_{in} and P_{out}.

The determined Wasserstein distance provides an adept measure of the collective difference in vegetation vitality between the nitrogen-fertilized (in-spot) and non-fertilized (out-spot) areas. A larger Wasserstein distance signifies that the application of nitrogen has a more pronounced impact on vegetation health and growth. Conversely, a smaller

distance indicates that the nitrogen application's effects are subtle or potentially overshadowed by other limiting factors. In essence, this metric aids in quantifying the tangible benefits of nitrogen application, allowing for more informed and sustainable agricultural decisions in the future.

Through this detailed analysis, we will identify which zones of the field have the most substantial response to nitrogen application, guiding future decisions on variable rate nitrogen application. This contributes towards the overarching goal of improving crop productivity, reducing nitrogen losses, and promoting sustainable agricultural practices.

3.10 Variable rate nitrogen application

With the in-depth comparison of in-spot and out-spot areas for each zone, we can now move towards the formulation of variable rate nitrogen application strategies. The zones demonstrating a more significant difference in their comparative analysis—meaning, where the in-spot showcased superior growth or a more positive response to nitrogen—are the ones that could benefit from an increased nitrogen rate during the top-dressing phase.

3.10.1 Utilization of comparative analysis information

The results of the comparative analysis, specifically the Wasserstein distance, serve as an effective indicator of each zone's responsiveness to nitrogen. Zones with a larger Wasserstein distance demonstrated a more profound growth improvement in the in-spot (where nitrogen was applied) compared to the out-spot (where nitrogen was not applied). Thus, these zones are more likely to benefit from additional nitrogen in the top-dressing phase.

3.10.2 Conversion of response indicator to nitrogen application rate

The next step is to translate this responsiveness indicator into a practical nitrogen application rate. For this purpose, we propose a linear scaling approach. The scaling

approach is intuitive and maintains the relative differences in responsiveness across zones.

In our analysis, we assign the symbol W_i to represent the Wasserstein distance for each specific zone, with 'i' serving as an index for the different zones. To establish a common scale, we identify W_{min} and W_{max} as the minimum and maximum Wasserstein distances observed across all zones. This allows us to normalize these distances into a uniform range of [0, 1], which is detailed in equation 3.9

$$W_i' = \frac{W_i - W_{\text{min}}}{W_{\text{max}} - W_{\text{min}}} \tag{3.9}$$

where W_i' represents the normalized Wasserstein distance for zone i.

The normalized Wasserstein distances, W_i', now provide a relative measure of each zone's responsiveness to nitrogen application, ranging from 0 (least responsive) to 1 (most responsive).

To ensure a balanced distribution of nitrogen across the zones, we further normalize the W_i' values using L1 normalization. This step adjusts the normalized values such that the sum of all W_i' across the zones equals 1. The L1 normalization is achieved as follows:

$$W_i'' = \frac{W'i}{\sum jW_j'} \tag{3.10}$$

where W_i'' represents the L1-normalized Wasserstein distance for zone i, and the denominator is the sum of all W_i' values across the zones.

This L1 normalization is crucial as it ensures that the total weight allocated to all zones sums up to 1, maintaining a proper proportional balance in nitrogen distribution. It ensures that the nitrogen application rates are not only reflective of each zone's responsiveness but also proportionate to the overall field requirements. This approach guarantees a more efficient and effective allocation of resources, optimizing nitrogen use across the entire field.

After obtaining the L1-normalized Wasserstein distances, W_i'', for each zone, the next step is to translate these relative responsiveness measures into concrete nitrogen application rates. This conversion is crucial for practical implementation in the field.

We achieve this by considering two key factors: the percentage area of each zone within the field and the total amount of nitrogen planned for application across the entire field. Essentially, each zone's final nitrogen application rate is a product of its relative responsiveness, its area proportion in the field, and the total nitrogen allocation for the field.

The calculation is as follows:

$$R_i = W_i'' \times \text{Area Percentage}_i \times \text{Total Nitrogen} \tag{3.11}$$

In this equation: R_i represents the final nitrogen application rate for zone i.
Area Percentage$_i$ is the proportion of the total field area that zone i occupies.
Total Nitrogen is the overall quantity of nitrogen designated for application across the entire field.

This method ensures that each zone receives a nitrogen application rate tailored to its specific needs and proportional to its area, aligning with the overall nitrogen budget for the field. It facilitates precise and efficient allocation of nitrogen, optimizing crop yield and minimizing waste or environmental impact.

3.11 Generating prescription maps

In parallel with drone-based image analysis, a similar process is applied to the satellite images obtained from the Sentinel platform. Here, the high-resolution multispectral images are subjected to the same analysis to calculate a separate nitrogen application rate. These satellite-derived rates, while generally less localized and detailed than the drone-derived rates, still provide an invaluable macroscopic perspective on nitrogen application.

Upon obtaining nitrogen application rates from drone imagery, satellite imagery, and historical field data, the next stage involves an integration process that weights these rates according to their relevance and reliability. This process involves assigning different importance weights to each of the three rates.

For instance, the drone-based analysis rate might be given a weight of 60%, recognizing the high level of detail, precision, and localization it offers. The historical field data, capturing long-term field responses, could be assigned a weight of 20%, while the satellite-derived rate could also receive a weight of 20%, reflecting its broader geographical perspective.

The weighting scheme, however, is not static and may need to be adjusted based on various situations. These could include the time of the season (early vs. late), the quality of the images obtained (cloud cover, shadows), the consistency between the drone and satellite rates, or the extent of deviations from the historical field data.

For instance, if cloud cover compromises the quality of satellite images, more weight might be given to the drone data and historical field data. On the other hand, if drone operations are interrupted due to technical issues, the weights might be adjusted to rely more on satellite data and historical records.

By dynamically adjusting these weights, we can ensure that the final nitrogen application rate reflects the best available information at any given time. This integrated and adaptive approach takes full advantage of the complementary strengths of drone imaging, satellite imaging, and historical data. It maximizes the precision and reliability of nitrogen application rates, paving the way for truly optimized, sustainable, and resilient crop production.

3.12 Harvesting and statistical analysis

Following the experiments, including procedures such as field scanning with EC, soil sampling, aerial photography, and image analysis, the subsequent phase involved

harvesting. This phase aimed to collect tangible samples from the field, providing evidence of our interventions' effects and highlighting contrasts among the various zones.

3.12.1 Sample collection and analysis

For each zone, samples are collected systematically to ensure the data is representative. The primary objective of this collection process is to understand the effects of interventions on yield and other essential metrics. Subsequent to collection, these samples undergo statistical analyses, facilitating the derivation of meaningful conclusions from the experimental data.

3.12.2 Graphical comparisons

To visualize the impact of the interventions, graphical comparisons are constructed. These comparisons aim to highlight disparities in yield and other essential metrics between the different zones and the control. Employing such visual aids provides a preliminary assessment tool for understanding the outcomes of the study.

3.12.3 Statistical tests

The t-test is a statistical method employed to determine if the means of two groups are statistically distinct from each other. This method aids in deciphering the probability that observed differences between groups are due to random variations. Within the scope of our study, the t-test is used to establish whether the variations discerned between the control and other zones are statistically significant, thereby strengthening the reliability of our outcomes.

The t-test operates on the following hypotheses:

Null Hypothesis (H_0): $\mu_1 = \mu_2$ (The means of the two groups are equal)

Alternative Hypothesis (H_a): $\mu_1 \neq \mu_2$ (The means of the two groups are not equal)

Where:

- μ_1 represents the mean of group 1 (for example, the Control zone).
- μ_2 stands for the mean of group 2 (such as any other zone).

The t-statistic, which measures the size of the difference relative to the variation in the data, is determined using Equation 3.12.

$$t = \frac{\bar{x}_1 - \bar{x}_2}{\sqrt{\frac{s_1^2}{n_1} + \frac{s_2^2}{n_2}}} \tag{3.12}$$

Here,

- $\bar{x}_1$ and $\bar{x}_2$ denote the sample means of the two groups.
- s_1^2 and s_2^2 are the sample variances for the two groups.
- n_1 and n_2 are the sample sizes for the two groups.

The p-value, which is the probability of observing a t-statistic as extreme as, or more extreme than, the statistic computed from the sample, given that the null hypothesis is true, is then procured from the t-distribution. A commonly used threshold is $p < 0.05$; if the p-value is below this, the null hypothesis is rejected in favor of the alternative hypothesis, signifying a significant difference between the two groups.

It merits emphasis that while statistical significance corroborates the existence of a distinction, it doesn't quantify the magnitude or direction of this variance. To bridge this gap, effect sizes were deduced using Cohen's d, a standardized metric designed to

measure the magnitude of differences between two groups. Cohen's d is derived as per Equation 3.13:

$$d = \frac{\bar{X}_1 - \bar{X}_2}{s_{\text{pooled}}} \tag{3.13}$$

Here, $\bar{X}_1$ and $\bar{X}_2$ signify the means of the two groups under comparison, while s_{pooled} represents the pooled standard deviation, a weighted mean of the standard deviations of the two groups. This pooled standard deviation is derived via Equation 3.14.

$$s_{\text{pooled}} = \sqrt{\frac{(n_1 - 1) \cdot s_1^2 + (n_2 - 1) \cdot s_2^2}{n_1 + n_2 - 2}} \tag{3.14}$$

In the equation, n_1 and n_2 stand for the sample sizes of the groups, while s_1 and s_2 indicate their respective standard deviations.

The values for Cohen's d can be interpreted as:

- **Magnitude**:
  - Small: —d— = 0.2
  - Medium: —d— = 0.5
  - Large: —d— = 0.8
- **Direction**:
  - A positive value of d suggests that the mean of the first group (e.g., the control group) is larger than the mean of the second group (e.g., a particular zone).
  - A negative value of d indicates that the mean of the second group (e.g., a particular zone) is larger than the mean of the first group (e.g., the control group).

3.12.3.1 Calculation of NUE based on protein content

The methodology for calculating NUE in wheat and corn production systems is predicated on the protein content of the grain yield. Protein content is a vital determinant of crop value and reflects the nitrogen assimilation efficiency of the plant, as proteins are composed of amino acids that contain nitrogen. The conversion of nitrogen to amino acids, and consequently to proteins, is indicative of the plant's ability to utilize applied nitrogen fertilizers for its growth and yield formation.

To compute the NUE based on protein content, the following formula is employed:

$$NUE = \left(\frac{(PC \times Y)}{AN + CN} \times N_c \right) \times UEF$$

where:

- PC is the Protein Content, given as a percentage of the harvested grain for each zone.
- Y represents the Yield, measured in pounds per acre (lbs/ac).
- AN denotes the Applied Nitrogen, the quantity of nitrogen fertilizer applied to the crop in lbs/ac.
- CN is the Credit Nitrogen, which accounts for the residual nitrogen available from the previous cultivation. In our wheat and corn fields, we consider the Credit Nitrogen to be 15 pounds per acre (lbs/ac), reflecting the typical nitrogen contribution of a soybean crop to the subsequent crop in the rotation.
- N_c is the Nitrogen Content factor in protein, which is typically 0.16 for wheat and corn, reflecting the nitrogen percentage in the protein [66], [74].
- UEF denotes the Utilization Efficiency Factor, which represents the fraction of nitrogen that is effectively utilized for grain protein production as opposed to other

plant growth aspects. While this factor can vary, for our analysis, we have considered a UEF of 50% for wheat and 35% for corn, based on established agricultural research and practices [7], [21], [87], [90]. .

This calculation framework allows for the assessment of the efficiency with which applied nitrogen is converted into the protein content of the grain. It forms the basis for comparing the effectiveness of nitrogen use across different agricultural zones.

4 Experimental results

4.1 Introduction

This chapter presents the experimental results obtained from studies conducted at two distinct fields in South Dakota. The first field, located at the SDSU Agricultural Experiment Station in Brookings, was cultivated with spring wheat. The second field, situated in Mount Vernon, was used for corn cultivation.

In the following sections, for each field, we will present:

- **Field information:** General information about the field.
- **Zones' Map:** A visualization obtained from soil EC scanning and sampling, demarcating the different zones.
- **Soil Features Breakdown:** An analysis of the inherent soil characteristics, particularly those pertinent to nitrogen dynamics.
- **AI-based Image Processing Insights:** Valuable findings extracted from drone and satellite imagery that mirror the actual field conditions.
- **Harvesting Sampling Insights:** Data procured from harvest samples, shedding light on crop health and yield.
- **Statistical Analyses:** Rigorous application of various statistical methods to the samples, reinforcing the validity of our results while also offering profound insights.
- **NUE Analysis:** An evaluation of the NUE in the crops, assessing how effectively the applied nitrogen contributes to the overall yield and productivity.

4.2 SDSU Agricultural Experiment Station

The SDSU Agricultural Experiment Station, located in Brookings, SD, is situated at coordinates 96°47'48.21"W longitude and 44°22'1.33"N latitude. In 2023, spring wheat

was planted at this location. In the following subsections, will provide a detailed exploration of our soil scanning results, image analysis, and various other experimental findings pertaining to this specific station.

Figure 4.1 complements our exploration by charting key experimental milestones alongside daily precipitation and temperature data for 2023. This includes critical phases like planting, EC scanning, soil sampling, establishing N-rich spots, drone imagery, top-dressing, and harvest times, offering insights into the environmental context of our research.

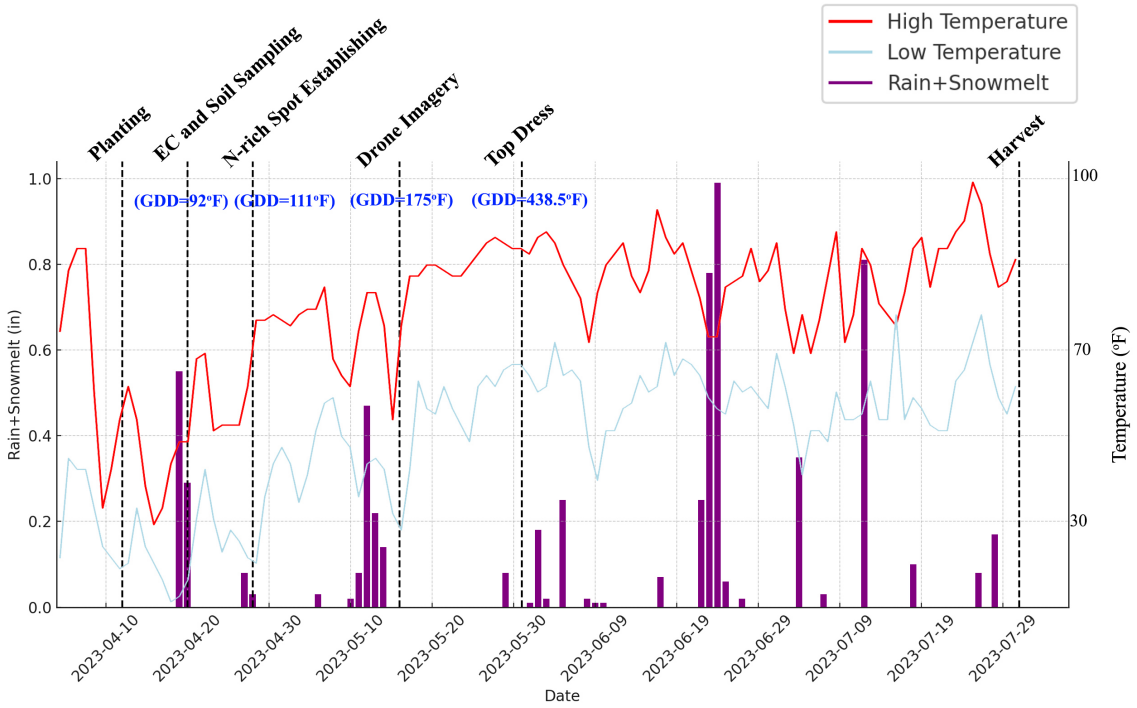

Figure 4.1: Experimental Timeline and Environmental Data: Illustrates key experimental events in 2023 at the SDSU Agricultural Experiment Station, including planting, EC scanning, soil sampling, N-rich spot establishment, drone imagery, top-dressing, and harvest. The chart juxtaposes these activities with daily precipitation, temperature, and Growing Degree Days (GDD) data, gathered from the Mesonet station in Brookings.

4.2.1 Soil EC and analysis results

Soil samples collected from this site underwent an analysis, revealing a combination of loam, clay loam, and silt clay loam soil types. The predominant clay loam presence highlights the field's ability to conserve moisture, bolster crop growth, and deter erosion. The presence of silt loam and loam further amplifies the field's fertility, creating prime conditions for crop cultivation. The zone map for this field, derived from EC scans and soil feature analysis, using the methodology described in section 3.2, is depicted in Figure 4.2. The soil sampling results focusing on Nitrate, Phosphate (P), Potassium (K), Organic Matter (OM), pH, and CEC can be found in table 4.1. Additionally, details about sand, silt, clay, and texture are presented in table 4.2.

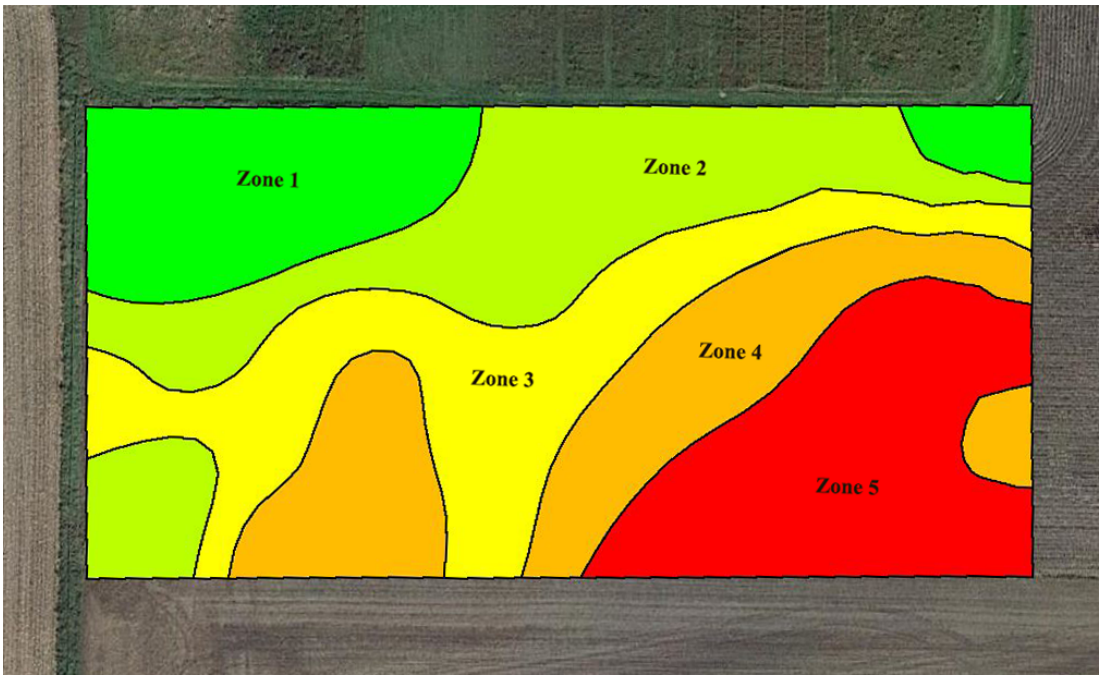

Figure 4.2: Zone Map of SDSU Agricultural Experiment Station field, extracted using EC scanning and soil features from soil analysis.

Table 4.1: Soil sampling results (part I) for SDSU Agricultural Experiment Station, Brookings, SD. The table provides details on the Nitrate, Phosphate, Potassium, Organic Matter, pH, and Cation Exchange Capacity of the soil samples.

Zone		**Nitrate**	**P**	**K**	**OM**	**pH**	**CEC**
Number	**Name**	ppm	ppm	ppm	%	**-**	cmol(+)/kg
1	Green	47	14	162	4.8	7.6	29.2
2	L-Green	190	20	145	4.4	6.5	3.6
3	Yellow	160	18	129	4.6	6.5	28.5
4	Orange	150	19	139	4.2	5.9	32.3
5	Red	110	15	117	4.4	6.5	22.5

Table 4.2: Soil sampling results (part II) for SDSU Agricultural Experiment Station, Brookings, SD: Soil Texture Information. The table provides details on the sand, silt, clay percentages, and soil texture.

Zone		**Sand**	**Silt**	**Clay**	**Texture**
Number	**Name**	%	%	%	-
1	Green	20	58	22	Silty clay loam
2	L-Green	26	45	29	Clay loam
3	Yellow	27	45	28	Clay loam
4	Orange	30	43	27	Clay loam
5	Red	31	46	23	Loam

4.2.2 Nitrogen response analysis

After analyzing the soil's intrinsic characteristics at the SDSU site, and establishing N-rich spots, the next critical component of our study involved studying the plant's response to nitrogen through image-derived techniques, as elucidated in the upcoming section. Utilizing the methodologies described in sections 3.5 to 3.11, we analyzed the plant's response to nitrogen application across different zones. The drone aerial photos were gathered on May 16, 2023, and satellite images gathered on May 27, 2023. Our

utilization of the Wasserstein distance method yielded quantitative measures of the differences in plant responses. This method ensured a nuanced understanding of how each zone reacted to different nitrogen application rates.

Table 4.3 presents a detailed breakdown of the results obtained:

- The area covered by each zone.
- The corresponding percentage of the field that each zone occupies.
- The normalized nitrogen response for each zone, derived from the Wasserstein distance method.
- The calculated percentage of nitrogen recommended for each zone based on our analysis.

Table 4.3: Detailed breakdown of nitrogen response in different zones obtained through image processing and the Wasserstein distance method, illustrating area coverage, normalized responses, and calculated nitrogen percentages.

Zone		**Area**	**Area**	**N Response**	**Response*Area**	**Dedicated N**
Number	Name	(ac)	%	%	-	%
1	Green	0.52	15.45	41.4	639.5	32.96
2	L-Green	0.811	24.10	31.3	754.9	38.94
3	Yellow	0.7	20.81	12.2	254.3	13.11
4	Orang	0.633	18.81	11.7	220.7	11.38
5	Red	0.7	20.81	3.4	69.7	3.7

4.2.2.1 Satellite data analysis

In addition to drone-based imagery, satellite data was also collected to analyze the field's response to nitrogen application. Two satellite images were captured on 5/27/2023 and 8/15/2023, respectively. Figures 4.3 and 4.4 present these satellite images.

Figure 4.3: Satellite image captured on 5/27/2023 showing the early stages of plant growth across different management zones in the field.

Figure 4.4: Satellite image taken on 8/15/2023 illustrating the matured plant growth and the discernible patterns across the management zones.

Comparing the satellite images with the drone-based images taken earlier on 05/16/2023, certain distinctions become evident. Despite the satellite images being captured at a later date, the drone images demonstrated superior results in terms of detailing the field's response. Specifically, the satellite images began to show the growth

pattern almost precisely only by 08/15/2023.

The limited resolution of the satellite images, at 10 meters, posed a challenge in differentiating between zones that did not exhibit highly distinguishable growth rates. This limitation is particularly pronounced due to the small size of the zones under observation. Considering these limitations, and after validating the drone imagery against the satellite data, it was determined that while both sources were utilized, greater emphasis was placed on the drone images due to their higher quality and detail.

4.2.2.2 Uniformity analysis of out-spot samples

As a natural extension of our image-derived analysis, we aimed to ascertain the uniformity of our out-spot samples, which serve as the control for the in-spot center. The results indicated a consistency across samples, marked by consistently low standard deviations. Such findings bolster the credibility of our control spots. Table 4.4 systematically catalogs the standard deviation values by zone for both NDVI and ExG metrics.

Table 4.4: Standard Deviation Values for Zone-Based Samples Compared with Control Spots.

Zone		**NDVI**			**ExG**		
Number	Name	Sample 1	Sample 2	Sample 3	Sample 1	Sample 2	Sample 3
1	Green	0.02	0.03	0.03	0.01	0.02	0.03
2	L-Green	0.03	0.02	0.02	0.02	0.01	0.03
3	Yellow	0.03	0.03	0.02	0.02	0.03	0.01
4	Orange	0.02	0.03	0.01	0.03	0.03	0.02
5	Red	0.03	0.01	0.02	0.01	0.02	0.03

4.2.3 Data integration and prescription map generation

Using the plant response patterns identified from image processing, we integrated these insights with historical data. This comprehensive analysis was designed to produce a

recommendation map for optimal nitrogen use in crops. This integration was essential in formulating a precise prescription map for nitrogen application. Our comparison with historical data allowed us to determine nitrogen application rates that optimize crop yields while maintaining environmental sustainability.

Table 4.5 outlines the synthesis of our findings with historical data for each zone:

- The historical nitrogen recommendation rates (HRR).
- Our AI-based computed rates, which were determined by multiplying the final nitrogen percentage (derived from image analysis) by the total nitrogen planned for field application.
- The integration of our findings with historical recommendations, given an 80-20 weighting. This weighting signifies that our image-derived rates were given 80% importance, while historical rates were attributed 20% importance.
- A final proposed nitrogen application rate, reduced by 16.2% from traditional recommendations, was determined based on our analytical findings. The decision to adjust the nitrogen application rates stemmed from a multifaceted consideration:
  - **Potential Yield Limitations**: After calculating the rates from our analysis, we juxtaposed them against the potential yield of each zone. Where the computed rates surpassed the zone's yield potential, we chose not to exceed the zone's natural limitation. By adhering to these potential yield thresholds, we ensure optimized resource allocation without overburdening the plants.
  - **Economic Considerations**: Applying nitrogen beyond the crop's absorption capacity does not just become futile in terms of yield improvement; it also leads to financial wastage. Oversupply of nitrogen does not correlate with a proportional increase in yield. Thus, maintaining rates that match the crop's actual needs ensures cost-effectiveness.

– **Environmental Impact**: Excess nitrogen that remains unabsorbed by crops can leach into the groundwater or runoff into nearby water sources. This not only poses a risk of water pollution but can also contribute to eutrophication, a process where water bodies receive excess nutrients leading to reduced oxygen and harm to aquatic life.

Considering the potential nitrogen uptake by plants, we have implemented a strategic reduction in nitrogen application by 16.2%. This adjustment entails a 20% decrease in application rates across all zones, with the exception of Zone 5. Due to its initially low rate, Zone 5 received an increase of 8 lbs./ac to meet the plants' nitrogen requirements adequately. Our approach balances the twin objectives of achieving optimal crop yields and minimizing environmental impact, while also being economically viable.

Table 4.5: Nitrogen application rates for different zones, comparing past recommendations with current rates adjusted for a 16.2% overall reduction in line with plant uptake potential. While a 20% decrease is uniformly applied to most zones, Zone 5 stands as an exception; it benefits from an additional 8 lbs./ac to satisfy plant nitrogen demands, highlighting our method's effectiveness in optimizing yields, ensuring sustainability, and maintaining economic efficiency.

Zone		**HRR**	**Drone-based rate**	**Data integration**	**Final rate**
Number	Name	(lbs./ac)	(lbs./ac)	(20%-80%)	(lbs./ac)
1	Green	80	98.88	95.1	76.08
2	L-Green	70	116.82	107.4	85.92
3	Yellow	60	39.33	43.46	34.77
4	Orang	50	34.14	37.31	29.85
5	Red	40	11.1	17	25.03

By converging our image analysis insights with field historical data, we derived a recommendation prescription map. This map suggests specific nitrogen application rates for each zone, epitomizing the outcome of our exhaustive analysis.

For this field, we utilized urea nitrogen labeled as 46-0-0. Given that this fertilizer comprises 46% nitrogen, the recommended rates, which are initially provided in lbs./ac of nitrogen, were adjusted. We divided the suggested amounts by 0.46 to calculate the appropriate quantity of actual nitrogen. Subsequently, to determine the actual quantity of urea nitrogen 46-0-0 required, we multiplied these adjusted numbers by the area of each respective zone. Additionally, the field's previous crop, soybean, has contributed a nitrogen credit of 15 lbs./ac to the soil.

4.2.4 Harvest data analysis

Upon developing a prescription map based on our analysis, we proceeded to evaluate the effectiveness of our nitrogen application strategies. The harvesting stage, described below, marked the conclusion of our study and provided an opportunity to observe the direct impact of our recommendations.

The harvesting stage began with a sampling strategy, shown in Figure 4.5. We designed our approach to collect a variety of samples from each zone while intentionally avoiding the N-rich spots. This was important as these areas had received a higher dose of nitrogen, and sampling them could bias our results.

Figure 4.5: Sampling strategy for harvesting time, illustrating the distribution of samples taken from each zone while avoiding N-rich spots. The design also highlights the uniform sampling approach employed in the control field across its various zones.

Building on the described approach, five samples were taken from each zone. Additionally, five unique samples were collected from the control section, where nitrogen was applied uniformly across the field. These samples were chosen to represent all the different zones within the control field. The combine harvester was instrumental in this phase, extracting samples from stripes each 24 feet (7.32 meters) long. As depicted in Figure 4.6, precision in the stripe length was maintained during the harvesting process, with an on-site researcher ensuring measurement accuracy.

Figure 4.6: Photograph of the combine machine in action during the sampling process, accompanied by a researcher ensuring the precise measurement of the 24-foot length sample stripe.

Following the sampling, the wheat samples were cleaned to remove impurities. Next, the samples were weighed to find out the yield. We then used a Foss Near-Infrared Spectroscopy (NIRS) analyzer to check the protein and moisture levels in the wheat samples.

Table 4.6: Average Wheat Yield Analysis by Zone: Comparing Weight (lb), Protein Content, Moisture Levels, Total Weight per Acre (lbs/ac), and Bushels per Acre (bu/ac) at SDSU's Seed Lab.

Zone		**Weight (lb)**	**Protein**	**Moisture**	**Yield**	**Yield**
Number	Name	(lbs.)	%	%	(lbs./ac)	(bu/ac)
0	Control	18.56	11.34	13.93	3502.64	58.39
1	Green	29.76	13.18	15.58	5610.34	93.44
2	L-Green	24.91	12.7	16.66	4697.32	78.29
3	Yellow	23.90	13.47	15.7	4510.64	75.25
4	Orange	22.74	12.72	15.02	4291.84	71.54
5	Red	19.34	12.34	14.66	3652.48	60.87

The total average yield for the entire field was 4505.25 lbs./ac or 75.09 bu/ac, assuming 60 lbs./bu for wheat. In contrast, the entire control field, which includes both the control spots and other areas, yielded about 66.61 bu/ac. Following the guidelines from SDSU Extension, the values were adjusted to a standard moisture content of 13%, ensuring it did not surpass 13.5% [11]. The complete analysis results can be found in Table 4.6.

4.2.5 Yield and protein content analysis

Following the harvesting and samples collection, we proceeded to a comparative analysis. This phase was imperative for evaluating the experimental zones in relation to a predetermined control, offering significant insights into the efficiency of our proposed approach.

4.2.5.1 Comparative analysis

A direct comparison between the experimental zones and the control reveals noteworthy differences. Zone 1 stands out with remarkable improvements. Other zones also exhibited

higher yields compared to the control, showcasing the effectiveness of the techniques applied. Zone 5 displayed results that were nearly identical to the control, showing a similar yield.

4.2.5.2 Graphical representation

To provide a clearer visual understanding of our findings, the next section presents a graphical representation. These visualizations are instrumental in accentuating the performance variations across zones. Figures 4.7 to 4.11 offer a graphical portrayal of the dataset, underscoring the disparities between the zones and the control. The visualizations reveals the performance of the zone 1 across the board, further corroborating the findings from the comparative analysis. Inclusion of the control zone in the visualizations (depicted in gray color) provides a direct visual baseline, making the discrepancies more palpable.

Delving deeper into the dataset, we observe the following relative to the control zone:

- **zone 1**: Showcases a remarkable increase in both protein content (approximately 16.23% higher) and yield (around 60.16% higher).
- **zone 2**: Exhibits approximately 12% higher protein content and 34.18% elevated yield.
- **zone 3**: While its protein content is about 18.78% more than the control zone, its yield sees a rise of roughly 28.74%.
- **zone 4**: Presents a protein content and yield that is approximately 12.18% and 22.50% higher than the control, respectively.
- **zone 5**: Even though its improvement in protein content is about 8.82% more than the control, the yield shows a modest increase of 4.17%.

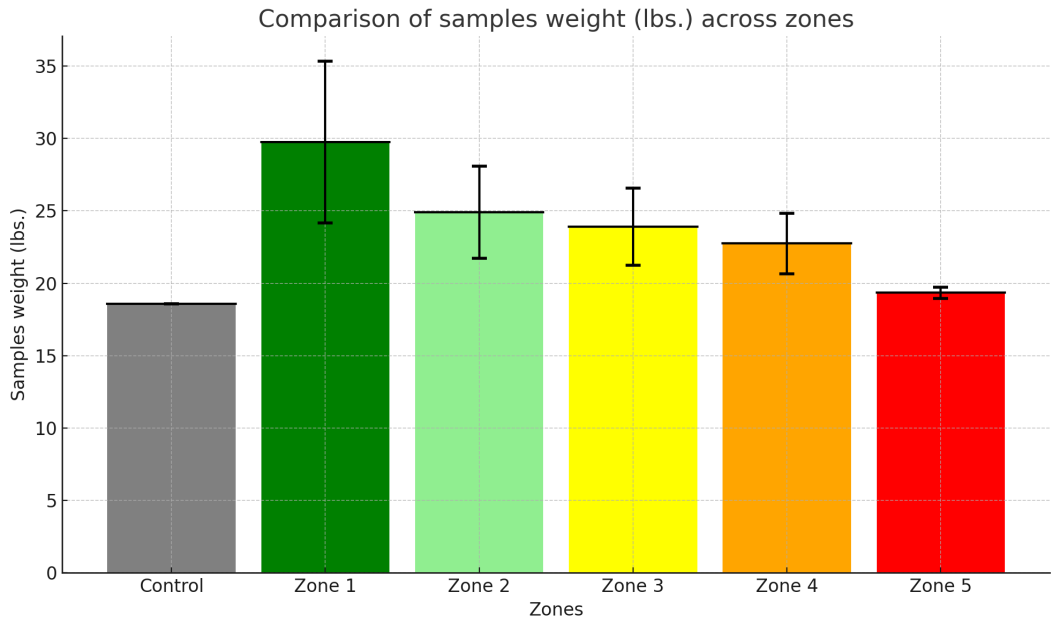

Figure 4.7: Comparison of sample weights in pounds across different zones in relation to the control. The error bars represent the standard deviation, highlighting the variation in sample weights from the control zone.

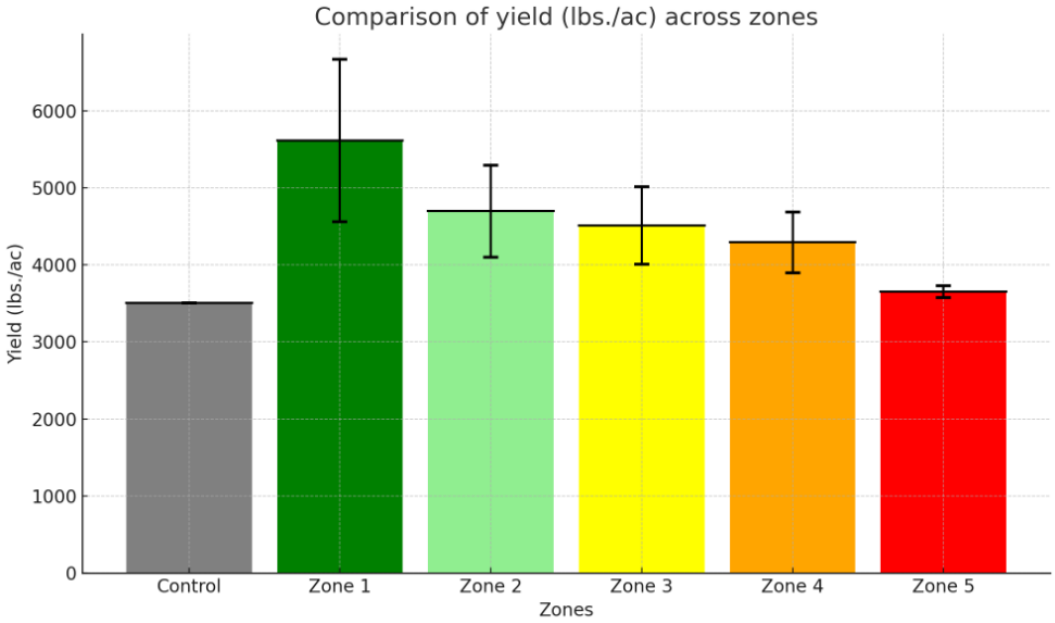

Figure 4.8: Comparison of yield measured in pounds per acre across different zones. The error bars denote the standard deviation, illustrating the discrepancies in yield (measured in pounds per acre) from the control zone.

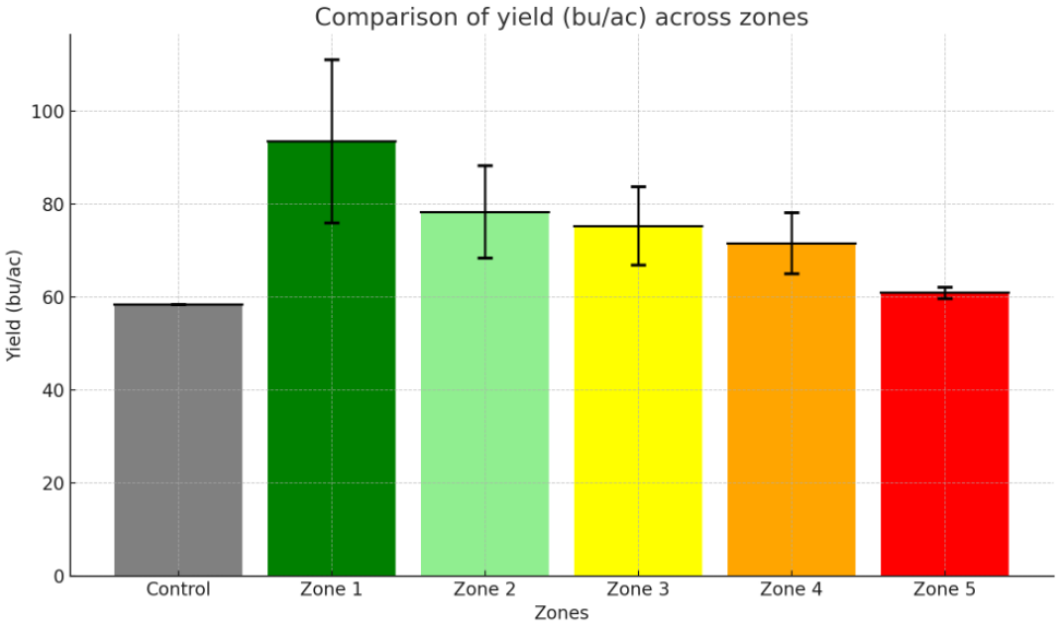

Figure 4.9: Comparison of yield measured in bushels per acre across different zones. The error bars showcase the standard deviation, indicating the variation in yield (measured in bushels per acre) from the control zone.

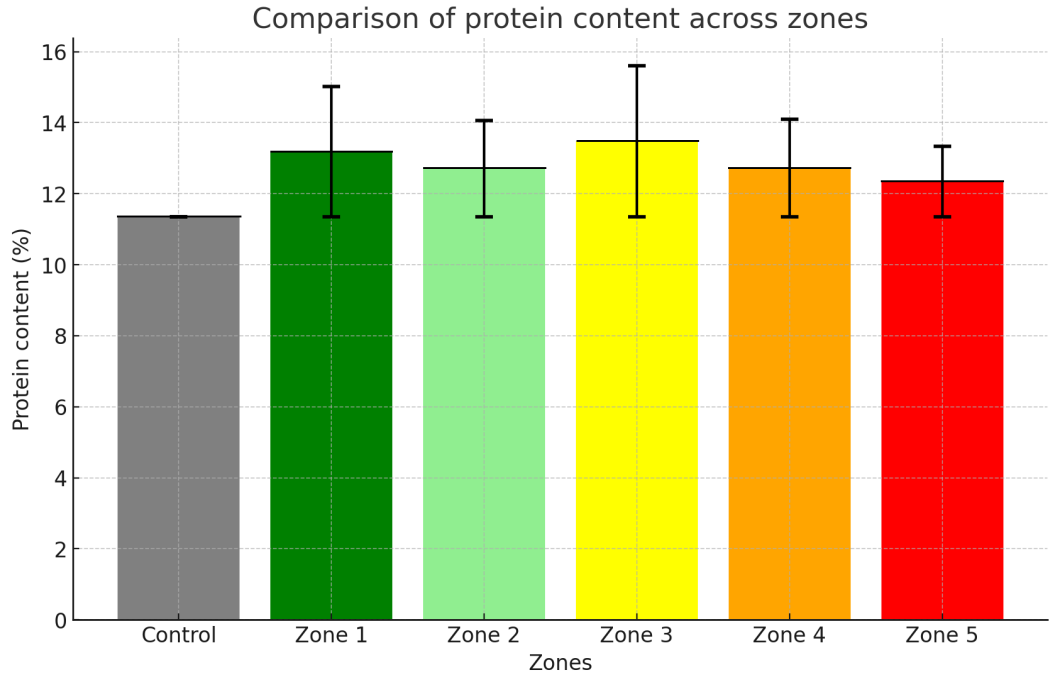

Figure 4.10: Comparison of Protein Content by Zone with Control: This figure illustrates the protein content variations in different zones relative to the control. Error bars indicate the standard deviation, emphasizing the extent of protein content variability from the control.

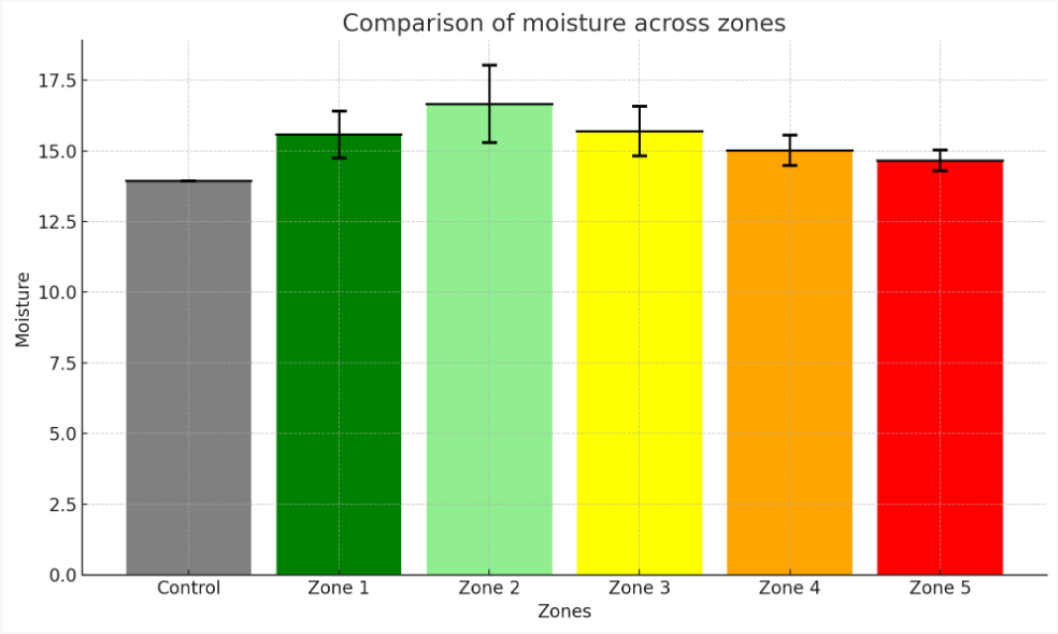

Figure 4.11: Comparison of moisture content across various zones with the control. The error bars represent the standard deviation, emphasizing the differences in moisture levels from the control zone.

4.2.5.3 Statistical significance via t-test

Building upon the comparative insights gleaned from the previous section, we further sought to assess the statistical significance of the observed differences between zones. To achieve this, a series of t-tests were conducted.

From the results, Zone 1 consistently demonstrated significant differences across all metrics when compared to the control. Specifically, weight metric revealed p-values that surpassed multiple levels of statistical significance.

Zone 2 also exhibited notable differences in weight metric, reaching levels of significance. Zone 3 showed significant disparities in weight metrics. In contrast, Zone 4 and 5 did not demonstrate any significant difference in weight metric when compared to the control.

In addition to the zonal analysis, a t-test comparison between the whole field and the control was conducted. The results indicate that the yield from our entire field was

75.09 bu/acre, while the control's yield was 58.39 bu/acre. Under a 95% confidence interval, our field's yield is approximately 28.28% higher than the control's yield.

The analysis reveals that under a 95% confidence interval, the yield from Zone 1 remains statistically distinct even when the control zone's yield increases by 22%. Similarly, for Zone 2, a yield increase in the control zone up to 12% still results in a statistically significant difference. For Zone 3, the threshold is a 7% increase in the control zone's yield. This indicates that, relative to the control zone, Zone 1 outperforms by 22%, Zone 2 by 12%, and Zone 3 by 7% in terms of yield.

Table 4.7 presents the p-values for each metric across different zones in comparison to the control zone. Various levels of significance are indicated with asterisks: $p < 0.001$ with "***", $p < 0.00$ with "**", and $p < 0.05$ with "*". These thresholds correspond to extremely significant, very significant, and significant levels, respectively, providing a nuanced understanding of the statistical outcomes.

Table 4.7: P-values and Confidence Levels for Zone Metrics Compared to Control: The p-values are denoted with significance codes — " for a confidence level of 99.9% (p ¡ 0.001), " for 99% (p ¡ 0.01), and " for 95% (p ¡ 0.05).

Zone		**Protein**	**Moisture**	**Weight**	**Yield (lbs./ac)**
Number	Name				
1	Green	0.0106**	0.0279*	0.0011***	0.0011***
2	L-Green	0.0757	0.0511	0.0052**	0.0052**
3	Yellow	0.2231	0.0123*	0.0134*	0.0135*
4	Orange	0.0097**	0.0064***	0.0569	0.0560
5	Red	0.1044	0.4206	0.5252	0.5152

To assess the magnitude and direction of the observed differences, we utilized Cohen's d as a measure of effect size, the results of which are detailed below.

Results: The effect sizes (Cohen's d) for the metrics with significant differences between zones and the control zone are as follows:

- **Green Zone**:
  - Weight: $d = -2.276$
  - Protein: $d = -1.634$
  - Moisture: $d = -1.356$
  - Lbs/ac: $d = -2.276$
  - Moisture-Normalized metrics: d values ranging from -2.281 to -2.293
- **L-Green Zone**:
  - Weight: $d = -2.388$
  - Lbs/ac: $d = -2.388$
  - Moisture-Normalized metrics: d values ranging from -2.406 to -2.407
- **Yellow Zone**:
  - Weight: $d = -2.004$
  - Moisture: $d = -2.035$
  - Lbs/ac: $d = -2.004$
  - Moisture-Normalized metrics: d values ranging from -1.987 to -1.999
- **Orange Zone**:
  - Protein: $d = -2.135$
  - Moisture: $d = -2.318$

Interpretation: The magnitude of the effect size, regardless of its sign (positive or negative), indicates the extent of the difference between the groups. Specifically, a large effect size, as denoted by the absolute value of Cohen's d, signifies a substantial difference between the groups. In the context of our study, the zones mentioned previously showed

pronounced differences in their respective metrics compared to the control zone. While the sign of the Cohen's d value provides directionality of the difference, the magnitude offers a more immediate sense of its importance. These specific Cohen's d values, therefore, provide a quantifiable measure of the magnitude of these differences, highlighting the significance of integrating both p-values and effect sizes for a holistic interpretation of the results.

These statistical outcomes, in conjunction with our comparative and graphical findings, further reinforce the efficacy and potential of our proposed method.

4.2.5.4 Comparative analysis of NUE across different zones

Following the methodology outlined in Section 3.12.3.1, we calculated the NUE for each of the five zones and entire field. The calculations were based on the protein content of the grain yield, the applied nitrogen, and the credit nitrogen from previous cultivation. These computations provide insight into the nitrogen conversion efficiency of each zone. The results of the NUE calculations are tabulated in Table 4.8.

Table 4.8: Comparison of NUE based on protein content for each zone and the entire field. The NUE variation values indicate the efficiency of nitrogen applied in contributing to the grain's protein content compared to the control zone.

Zone		**NUE**	**NUE variation from control**
Number	Name		
1	Green	0.649	0.160
2	L-Green	0.472	-0.015
3	Yellow	0.976	0.488
4	Orange	0.973	0.485
5	Red	0.90	0.412
-	Control	0.488	-
-	Entire Field	0.650	0.162

From the results, it is evident that the nitrogen application strategy significantly impacted the protein content and thus the NUE across different zones. Most zones outperformed the control in terms of NUE, indicating a more efficient conversion of applied nitrogen into protein content in the grain. Zone 2 (L-Green), however, exhibited a lower NUE compared to the control. This anomaly can be attributed to the highest rate of nitrogen application within this zone, suggesting that a portion of the nitrogen may not have been effectively utilized in synthesizing protein within the grain. The entire field's NUE closely mirrored that of the control, reflecting an overall balanced nitrogen usage when considering all zones collectively.

4.3 Mount Vernon, SD

The second field under consideration is situated in Mount Vernon, SD, at coordinates 98°18'41.99"W longitude and 43°44'59.27"N latitude.This field spans 135.54 acres. In 2023, this field, provided by a local farmer, was selected for the cultivation and study of corn. The subsections below will detail our findings.

Figure 4.12 presents a crucial timeline charting the 2023 experimental activities in the Mount Vernon field. This visualization helps contextualize the environmental conditions during key phases like planting, EC scanning, soil sampling, establishing N-rich spots, and drone imagery capture.

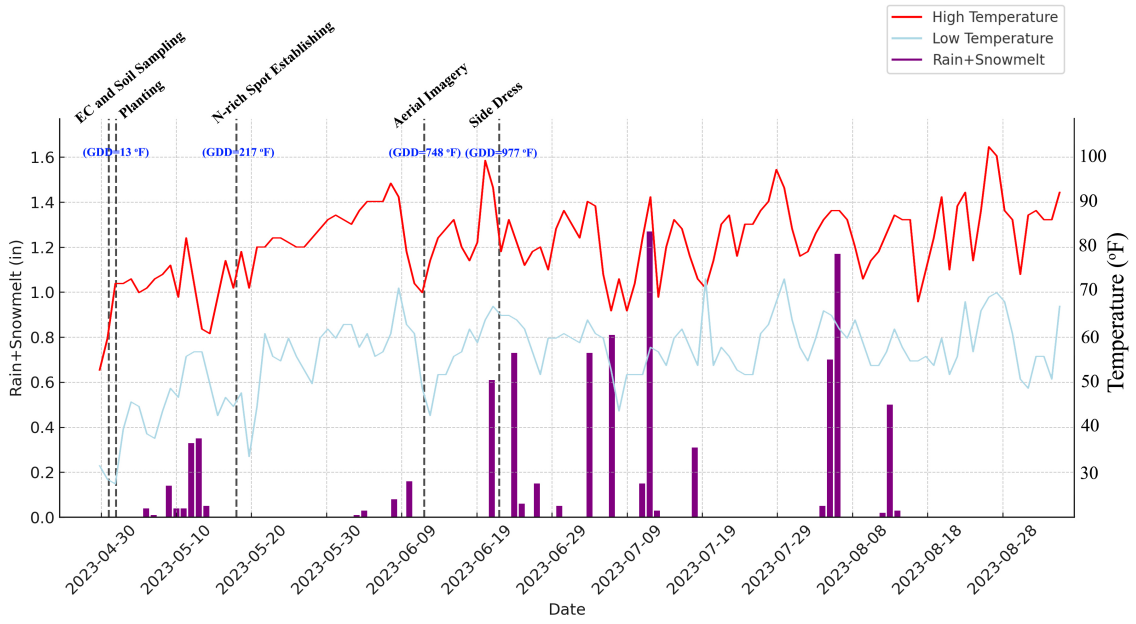

Figure 4.12: Experimental Timeline and Environmental Data: Illustrates key experimental events in 2023 at the corn field, including planting, EC scanning, soil sampling, N-rich spot establishment, drone imagery, and side-dressing. While harvest day on November 1 is not depicted in the chart for readability, its timing is critical in understanding the study's outcomes. The chart juxtaposes these activities with daily precipitation, temperature, and Growing Degree Days (GDD) data, gathered from the Mesonet station in Mount Vernon, SD.

4.4 Soil EC and analysis results

The soil in this region is composed of silty loam, loam, and sandy loam. The soil exhibits diverse nitrate and phosphate levels, underscoring the necessity for precise nutrient management. Figure 4.13 displays the zone maps of Mount Vernon, derived from EC scans and soil features represented in Table 4.9 and Table 4.10.

Figure 4.13: Zone Map of Mount Vernon field, extracted using EC scanning and soil features from soil analysis.

Table 4.9: Soil Sampling Results (Part I) for Mount Vernon field. The table provides details on the Nitrate, Phosphate, Potassium, Organic Matter, pH, and Cation Exchange Capacity of the soil samples.

Zone		**Nitrate**	**P**	**K**	**OM**	**pH**	**CEC**
Number	**Name**	ppm	ppm	ppm	%	**-**	cmol(+)/kg
1	Green	250	12	180	2.7	7.4	26.3
2	L-Green	150	11	203	2.4	7.5	22.3
3	Yellow	220	40	313	2.7	5.1	40.8
4	Orange	93	24	220	2.8	5.3	28.5
5	Red	71	21	417	3.9	5.5	23.2

Table 4.10: Soil Sampling Results (Part II) for Mount Vernon field: Soil Texture Information. The table provides details on the sand, silt, clay percentages, and soil texture.

Zone		**Sand**	**Silt**	**Clay**	**Texture**
Number	**Name**	%	%	%	-
1	Green	27	56	17	Silty loam
2	L-Green	46	35	19	Loam
3	Yellow	43	39	18	Loam
4	Orange	47	37	16	Loam
5	Red	57	35	8	Sandy loam

4.4.1 Prescription map generation

Following the methodology applied at the SDSU site, we first established management zones and N-rich spots in the Mount Vernon field, which are depicted in Figure ??. Subsequently, we analyzed the plant's response to nitrogen through AI-based image processing techniques. We integrated the analysis results from drone and satellite images, and historical recommendation rates to generate the final prescription map, as outlined in Table 4.11 and Table 4.12.In the data integration process, the historical nitrogen application rate of the field was weighted at 20%, while recommendations from drone-based image analysis were given a 70% weight, and results from satellite-based image analysis were accounted for at 10%. Considering plant's N uptake and growth potential, we decided to reduce nitrogen application by 10% for this field.

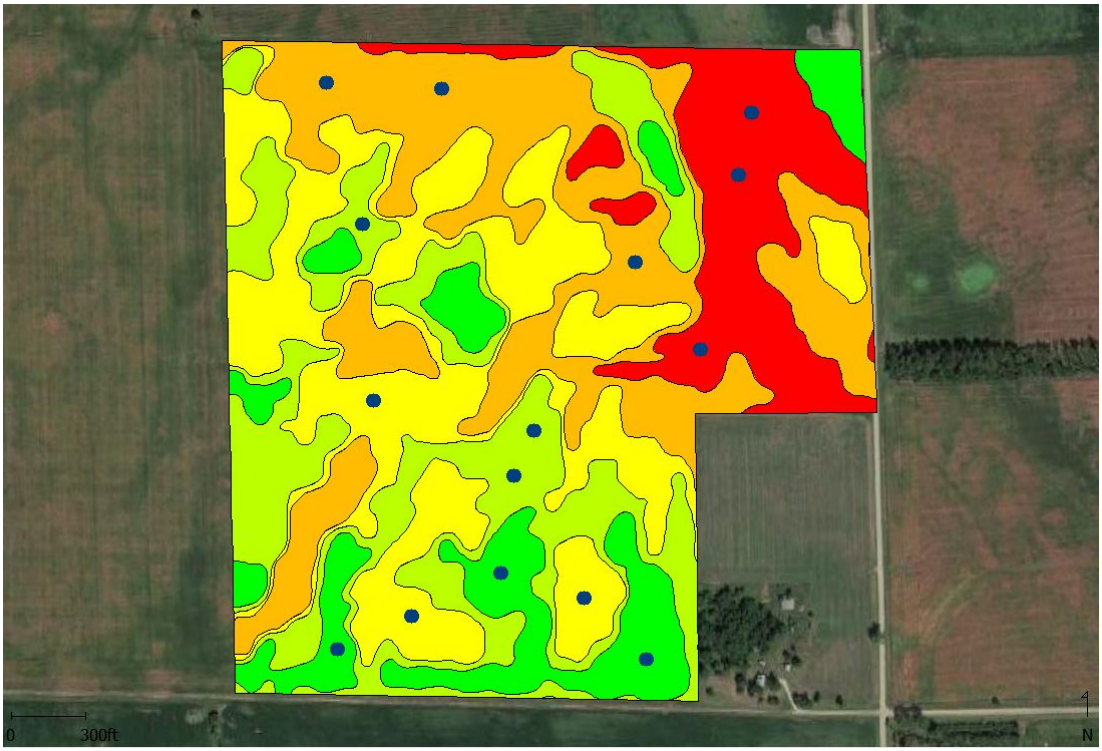

Figure 4.14: Zone Map of the Mount Vernon Field Highlighting Established N-Rich Spots. Three spots are placed within each zone to ensure representation of field conditions.

Table 4.11: Nitrogen application rates by zone, detailing historical recommendations and computed rates from drone and satellite image analysis.

Zone		**HRR**	**Satellite-based Rate**	**Drone-based Rate**
Number	Name	(lbs./ac)	(lbs./ac)	(lbs./ac)
1	Green	75.9	29.9	50.78
2	L-Green	64.4	64.4	43.64
3	Yellow	52.9	52.9	60.03
4	Orange	41.4	41.4	57.19
5	Red	29.9	75.9	51.84

Table 4.12: Results of data integration and proposed nitrogen application rate reduction for optimization.

Zone		**Data integration (20-10-70)**	**10% Reduction**
Number	Name	(lbs./ac)	(lbs./ac)
1	Green	53.71	48.34
2	L-Green	49.86	44.88
3	Yellow	57.89	52.10
4	Orange	53.15	47.83
5	Red	49.85	44.87

Contrary to expectations based on historical data and zone maps, our approach revealed some surprising findings. While zone 5 was anticipated to exhibit the lowest growth rate and consequently the lowest yield, our analysis indicated a higher-than-expected growth rate in this zone. A similar trend is observed in other zones as well. This discrepancy could be attributed to various factors such as the zone's drainage capability, rainfall, among others. Notably, our approach identified this deviation, unlike traditional methods that rely solely on historical data. Figure 4.15 illustrates this inversion, showcasing an image that represents the growth rate in different parts of the field. The image, with varying shades of green, indicates the plants' response to nitrogen, with more vibrant green signifying better growth and a positive response to nitrogen application.

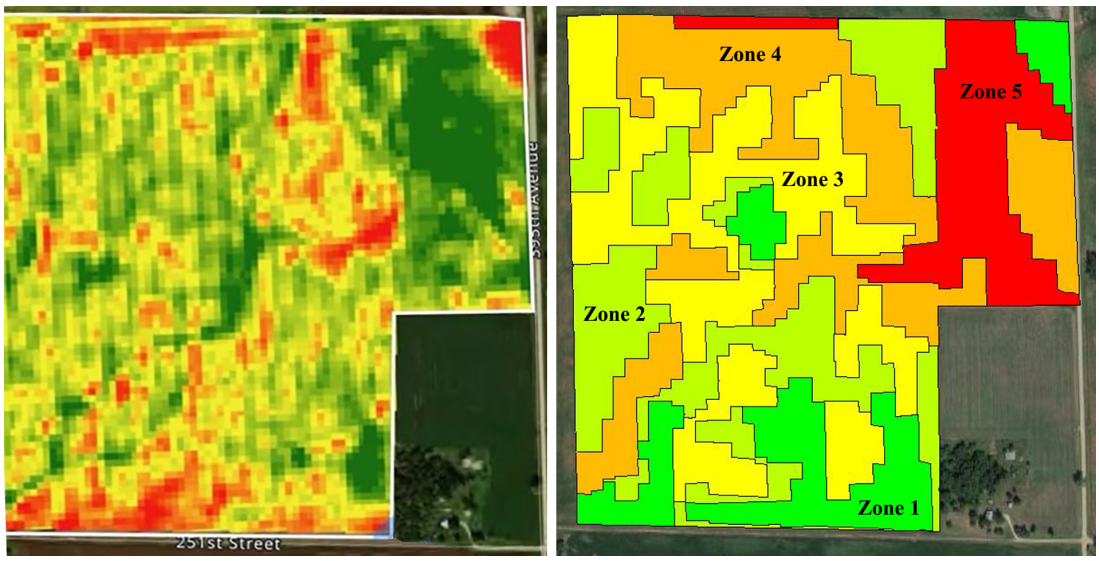

Figure 4.15: Comparison of plant response to nitrogen and traditional expectations. On the left, the computed growth rate, indicated by varying shades of green (with darker green signifying better growth), showcases the plant's response to nitrogen based on our analysis. On the right, the management zones depict expectations from traditional approaches.

As indicated in Table 4.12, due to the collaborative nature of this project with a local farmer and the constraints in operational farming, we incorporated the field's historical nitrogen application data alongside our analytical findings into the nitrogen management strategy. To validate our approach, we established replicated test strips across the field. Each strip was divided into four plots, with each plot receiving a distinct nitrogen application rate that blends the farmer's historical practices with our recommendations. This approach allowed us to observe the impact of varying nitrogen rates on crop performance. These replicated strips were designed to represent the variability within each zone adequately. The specific nitrogen application rates for each plot within the strips are detailed in Table 4.13, and the layout of these test strips is depicted in Figure 4.16.

Figure 4.16: Layout of the nitrogen application test strips in the Mount Vernon field. Each strip is segmented into four plots, with each plot receiving a unique nitrogen application rate to assess the impact on crop performance. The strips are replicated across each zone to ensure representation of the field's variability.

Table 4.13: Nitrogen application rates for each plot within the test strips, applicable to all zones.

Plot		**N application rate**
Number	Name	(lbs./ac)
1	Green	57
2	L-Green	46.5
3	Yellow	43.8
4	Red	34.5

4.4.1.1 Uniformity analysis of out-spot samples

Similar to the analysis conducted for the SDSU field, we assessed the uniformity of out-spot samples in the Mount Vernon field. These samples acted as controls for the in-spot centers in analyzing plans' response to N application. Our findings showed uniformity, with low standard deviations across samples, reinforcing the reliability of our control spots. The uniformity data, including standard deviation values for NDVI and ExG metrics by zone, is detailed in Table 4.14.

Table 4.14: Standard Deviation Values for Zone-Based Samples Compared with Control Spots.

Zone		**NDVI**			**ExG**		
Number	Name	Sample 1	Sample 2	Sample 3	Sample 1	Sample 2	Sample 3
1	Green	0.03	0.04	0.02	0.05	0.03	0.01
2	L-Green	0.02	0.02	0.04	0.02	0.02	0.02
3	Yellow	0.02	0.04	0.02	0.02	0.03	0.01
4	Orange	0.02	0.02	0.03	0.04	0.01	0.02
5	Red	0.04	0.01	0.02	0.03	0.02	0.01

4.4.2 Yield data analysis

In contrast to the sampling approach employed at the SDSU field, the Mount Vernon field benefited from the use of a high-tech combine harvester equipped with yield monitoring capabilities. This allowed for real-time yield data collection during the harvest, providing precise yield measurements for each management zone and individual strip plot.

4.4.2.1 Comparative analysis

Table 4.15 details the yield data, standardized to a moisture content of 15%, and displays the applied nitrogen rates for each zone and plot. Prior to analysis, the yield data underwent a thorough data cleaning process to ensure accuracy and reliability of the results.

Table 4.15: Yield and Applied Nitrogen Rates for Each Zone and Plot, Adjusted for 15% Moisture Content.

Zone		**Strip**	**Applied N**	**Yield**
Number	Name	-	(lbs./ac)	(bu/ac)
Zone 1	Green	control	48.34	164.4
		strip 1	57	166.71
		strip 2	46.5	163.9
		strip 3	43.8	163.5
		strip 4	34.5	159.19
Zone 2	L-Green	control	44.88	165.69
		strip 1	57	171.12
		strip 2	46.5	166.55
		strip 3	43.8	166.47
		strip 4	34.5	165.45
Zone 3	Yellow	control	52.1	168.36
		strip 1	57	173.75
		strip 2	46.5	173.85
		strip 3	43.8	165.27
		strip 4	34.5	160.53
Zone 4	Orange	control	47.83	167.19
		strip 1	57	175.37
		strip 2	46.5	170.46
		strip 3	43.8	173.69
		strip 4	34.5	165.21
Zone 5	Red	control	44.84	167.46
		strip 1	57	182.14
		strip 2	46.5	178.54
		strip 3	43.8	171.99
		strip 4	34.5	158.48

The yield analysis across the zones, excluding the strip areas, demonstrates varied productivity levels. Zone 3 yielded the highest at 168.36 bu/ac, while Zone 1 had the lowest yield at 164.4 bu/ac. The aggregated data from these zones resulted in an average field yield of 166.86 bu/ac.

4.4.2.2 Graphical representation

To visually compare the yield across different zones and test strips, we first juxtaposed each zone and its strips against the field's average yield. Figure 4.17 includes error bars that reflect the variance of each zone/strip from the field's average yield. Additionally, Figures 4.18 through 54.22 individually illustrate the yields of each zone with their respective strips, where error bars represent the yield deviation between the zone's control and its strips.

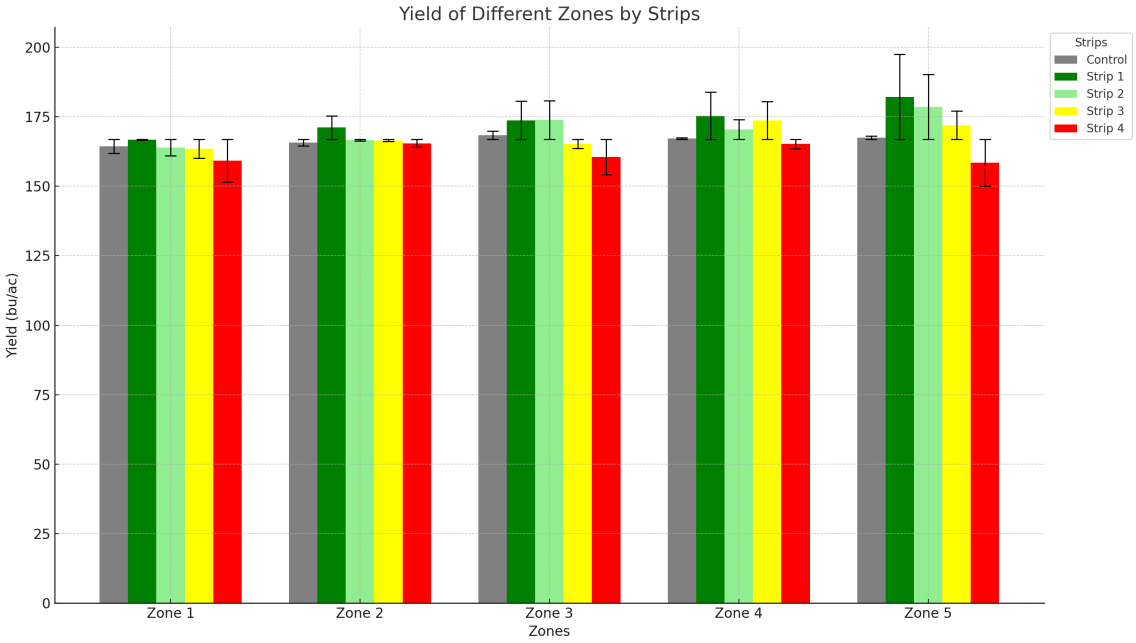

Figure 4.17: Yield comparison across five agricultural zones with varying nitrogen strip treatments. Each zone is represented by a series of bars, each color-coded to denote a different strip treatment: control (gray), strip 1 (green), strip 2 (light green), strip 3 (yellow), and strip 4 (red). The yield values are measured in bushels per acre (bu/ac) and presented along the y-axis. T-shaped error bars indicate the deviation of each strip's yield from the reference value of 166.86 bu/ac which represents averaged field yield.

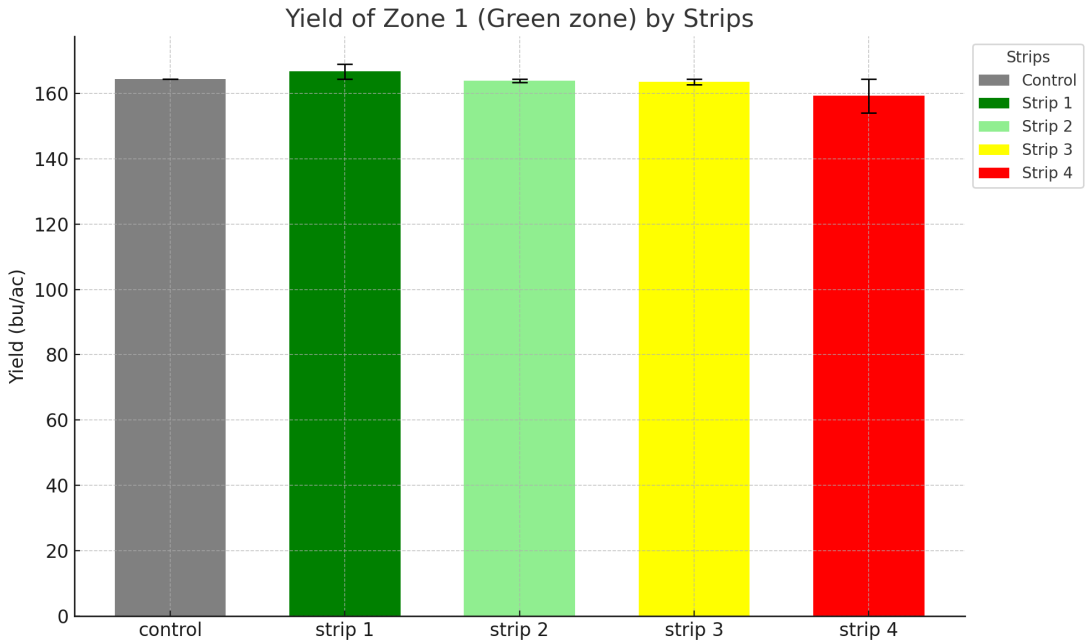

Figure 4.18: Illustrating the yield results for Zone 1, identified as the Green zone, displaying the yield variations across five different strip treatments. Error bars represent the deviation of each strip's yield from the control within this zone.

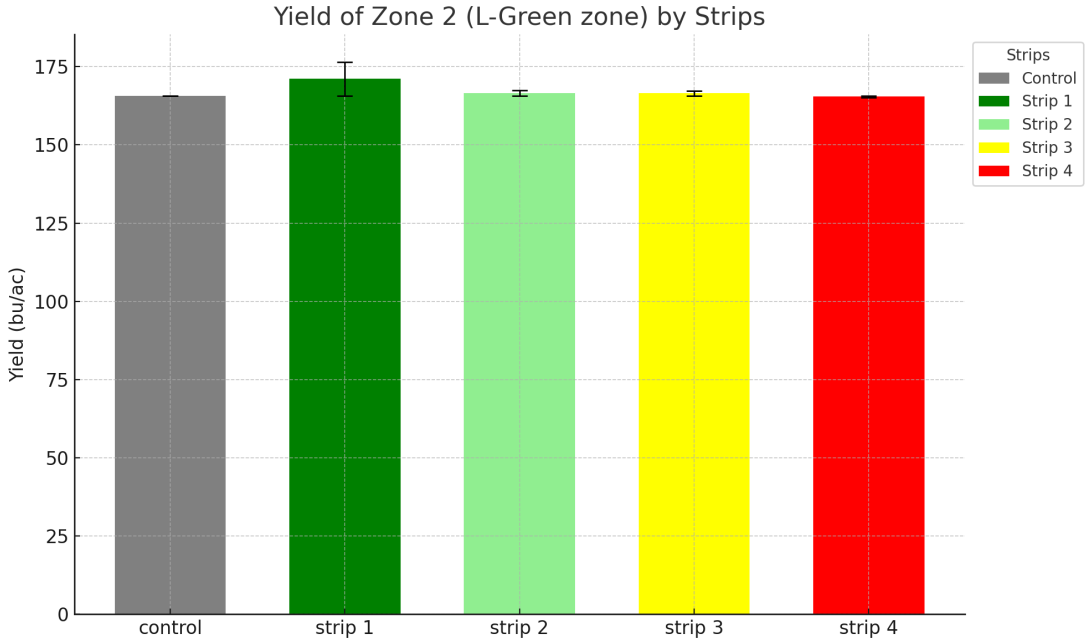

Figure 4.19: Presenting the yield performance in Zone 2, the L-Green zone, with each bar representing one of five strip treatments. The error bars indicate the difference in yield compared to the zone's control strip.

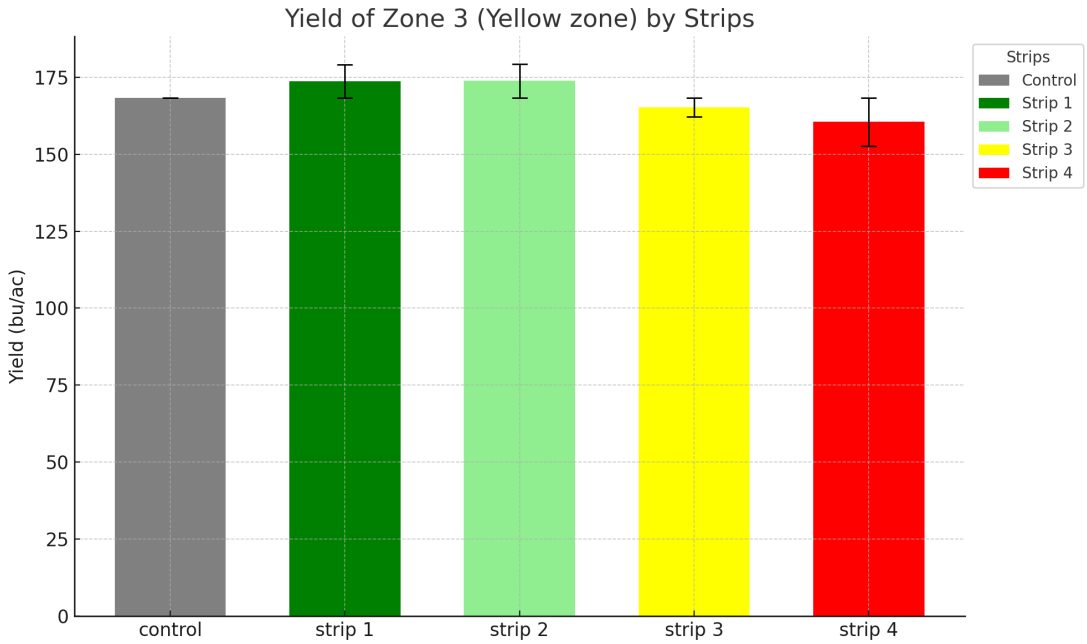

Figure 4.20: Depictsing the yield comparison within Zone 3, known as the Yellow zone, highlighting the yield outcomes for each strip treatment relative to the control. Error bars provide a measure of each strip's yield fluctuation from the control.

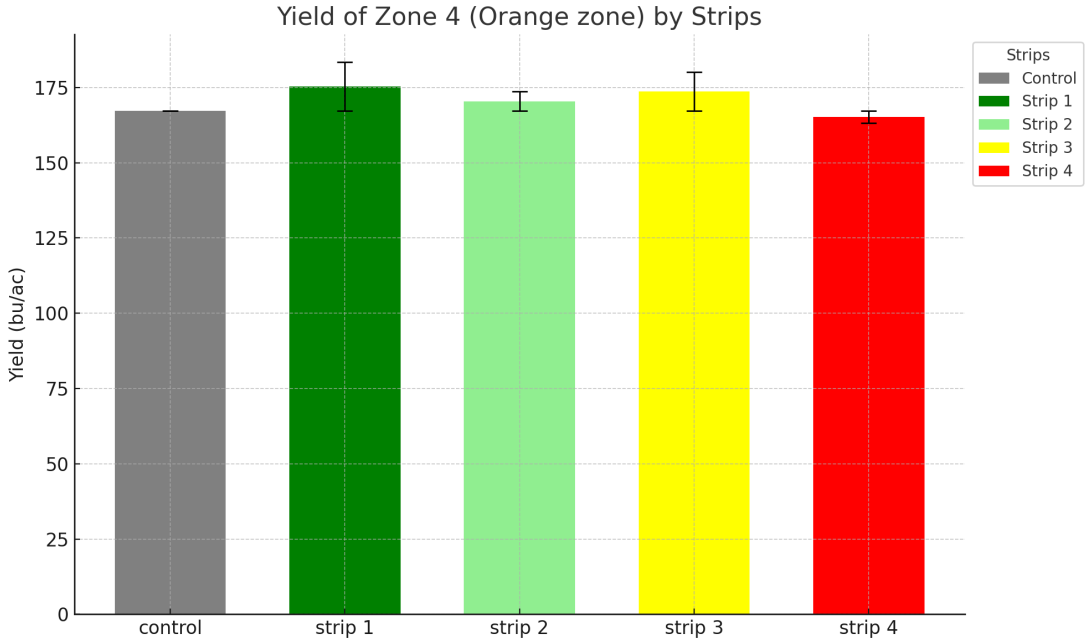

Figure 4.21: Showing the yield data for Zone 4, termed the Orange zone, with each bar denoting the yield for a specific strip treatment. The error bars visualize the yield variance of each strip from the control's yield within the zone.

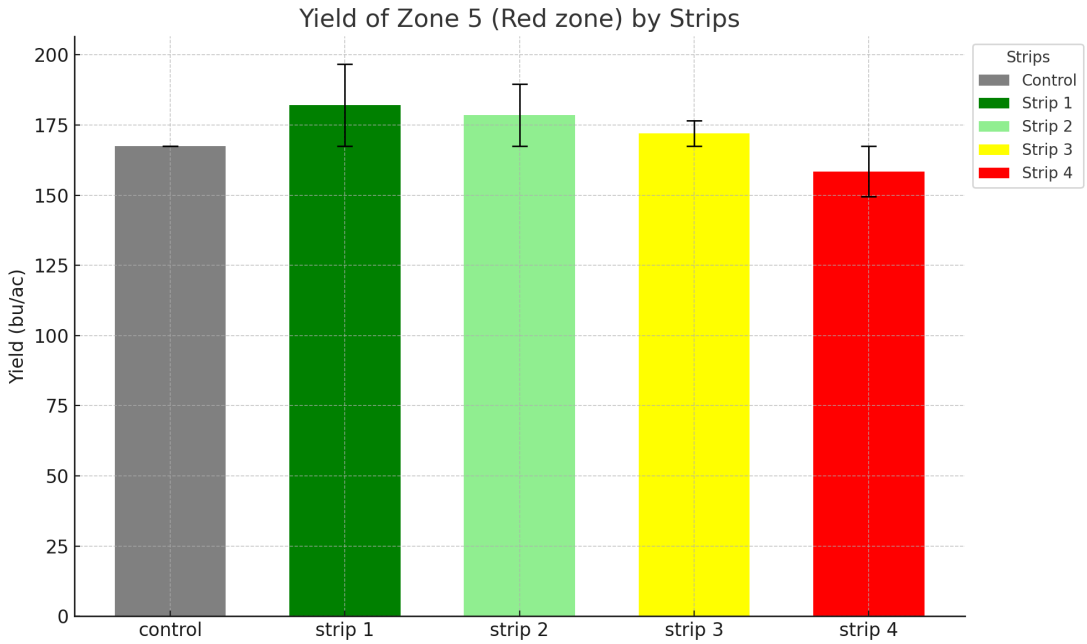

Figure 4.22: Displaying the yield analysis for Zone 5, designated as the Red zone, comparing the yield across different strip treatments. The error bars reflect how much each strip's yield deviates from that of the control strip in the zone.

4.4.3 Comparative yield estimations

In this section, we evaluate the outcomes of different nitrogen application strategies to determine the most effective approach for yield and nitrogen optimization. Specifically, we compare the average field yield resulting from adherence to the farmer's historical recommendations against yields derived from our AI-based drone and satellite image analyses. To facilitate this comparison, we utilized linear regression to interpret the data collected from our field experiments.

Our field experiment was designed with four strips per zone, each replicated to enhance the reliability of our findings. Within each strip, four distinct plots were treated with different nitrogen application rates, as shown in Figure 4.16. This design allowed us to isolate the effects of nitrogen application based on our AI-driven image analysis, independent of the farmer's historical recommendations.

The regression analysis, based on the nitrogen application rates outlined in Table

4.11, shows distinct yield outcomes as follows:

- Adhering strictly to the farmer's historical rates would result in an average yield of 165.84 bushels per acre.
- Following only the drone-based image analysis recommendations would lead to an average yield of 173.75 bushels per acre.
- Relying solely on satellite-based image analysis would yield an average of 172.54 bushels per acre.

These results are compared against an actual yield of 166.86 bushels per acre, achieved by integrating all three approaches (historical, drone-based, and satellite-based). Interestingly, each individual method projects higher yields than farmer's historical based approach. Specifically, the deviations from the integrated yield are -0.61% for the farmer's rate, +4.13% for the drone-based, and +3.40% for the satellite-based method. This comparison highlights that our AI-based approaches are more effective than farmer's rate.

After conducting a t-test to compare each approach with the baseline integrated yield of 166.86 bushels per acre, we found significant statistical differences. Notably, the drone-based approach, with an average yield of 173.75 bushels per acre, demonstrated a statistically significant difference from the baseline (p ¡ 0.05). This suggests that the drone-based method's yield improvement is not due to random variation but is a reliable deviation from the integrated approach. In contrast, the farmer's and satellite-based methods did not show a statistically significant difference from the baseline yield.

4.4.3.1 Comparative analysis of NUE for different methodologies

Following the steps in Section 3.12.3.1, we calculated the NUE for different fertilization strategies in our field study. These strategies included the farmer's usual nitrogen application, analysis from drone and satellite images, and the integrated approach, which served as our baseline for comparison. Lacking specific protein content data for this field,

we used the average corn grain protein content of 8.5% as cited by the SDSU Extension [97]. The calculated NUE values, listed in Table 4.16, represent the effectiveness of each strategy as a percentage relative to our baseline, the integrated method, taking into account the total field yield and the differing amounts of nitrogen applied per strategy.

Table 4.16: NUE comparison across fertilization strategies relative to the integrated approach, considering total field yield and applied nitrogen. NUE percentages demonstrate the effectiveness of each strategy in improving grain protein content taking into account the amount of nitrogen applied.

Fertilization Strategy	**NUE**	**NUE Variation from Baseline**
Integrated approach (baseline)	0.926	-
Farmer's usual nitrogen application	0.921	- 0.005
Satellite images-based	0.958	0.031
Drone images-based	0.965	0.038

The table provides a clear comparison of NUE variations among different fertilization strategies, with the integrated approach serving as a reference standard. Notably, the farmer's usual nitrogen application method resulted in a negative NUE variation of -0.005. This suggests that the farmer's method did not translate into a proportional increase in yield's protein content. In contrast, strategies based on satellite and drone images showed positive NUE variations, at 0.031 and 0.038 respectively, demonstrating that these AI-driven methods surpassed the yield achieved by the farmer's traditional approach. This highlights the potential of technology-enhanced practices to optimize resource use and improve crop outcomes.

4.5 Faster R-CNN model performance evaluation

After the training process, our model achieved a high level of performance. Specifically, the model reached a training accuracy of 98.5%. The slight inaccuracies primarily arose from images taken from higher altitudes, where the tiles appeared smaller and less

distinct. Further, variations in tile color due to wear and occasional occlusions from shadows or debris also contributed to these minor errors.

During the validation phase, the model demonstrated a validation accuracy of 97.2%. This assessment was crucial to ensure that the model was generalizing well, beyond merely memorizing the training data.

Finally, in the testing phase, the model exhibited a testing accuracy of 96.8%. This performance provides a robust indication of the model's capabilities, confirming its preparedness for real-world applications and deployment.

In addition to accuracy, we evaluated the model using Precision, F1 Score, and Intersection over Union (IoU). Table 4.17 summarizes these metrics across different phases of the model evaluation:

Table 4.17: Performance metrics of the Faster R-CNN model

Metric	**Training**	**Validation**	**Testing**
Accuracy (%)	98.5	97.2	96.8
Precision (%)	96.7	95.4	94.9
F1 Score (%)	97.6	96.3	95.8
IoU (%)	92.3	90.5	89.7

4.6 Outcomes

4.6.1 Environmental outcomes

In a research conducted on wheat and corn fields, nitrogen was variably applied to distinct management zones, customized to match the plants' nitrogen uptake capacity. Over-application of N may result in leaching nitrogen into groundwater, while under-application can reduce the production efficiency. This research demonstrated a strategy that optimize the application rate with plant requirements considering environmental sustainability.

4.7 Financial outcomes

The study implemented a method that tailored the application of nitrogen fertilizer to the plant's needs in different management zones, leading to a 16.2% reduction in usage on a 3.36-acre wheat field. With the nitrogen price of $0.68 per pound of nitrogen content [96], this reduction resulted in a cost saving of $26.45 for the entire 3.36-acre field, or potentially $7.87 per acre. If this approach were applied to a larger field of 1,000 acres, the estimated savings could potentially be $7,870.00. In the corn field, spanning 135.54 acres, our method reduced nitrogen application by 10%, equating to a decrease of 5.33 lbs./ac of nitrogen. Given the same nitrogen prices, this reduction translates to a savings of potentially $3.62 per acre. For the entire 135.54 acres, the total cost savings would be $491.25. Extrapolating these savings to a 1,000-acre corn field, the method could potentially save $3,624.40 in nitrogen costs.

Concurrently, the study examined wheat yields from both a test field and a control field. The test field, utilizing the novel agricultural methodology, yielded 75.09 bu/ac, while the control field yielded 66.61 bu/ac. Statistical analysis at a 95% confidence interval indicated that the yield from the test field was potentially 12.40% higher compared to the control field. In a similar vein, the research extended to a corn field where an integrated method served as the baseline. This method, a combination of farmer's rate, satellite-based rate, and drone-based rate as described in Table 4.12, yielded 166.86 bu/ac. The farmer's approach yielded slightly less at 165.84 bu/ac, representing a minor decrease of approximately 0.61% from the baseline yield of 166.86 bu/ac, rather than an increase. The satellite-based approach, on the other hand, resulted in a yield of 172.54 bu/ac, surpassing the baseline by approximately 3.4%. Even more impressive was the drone-based method, which achieved the highest yield of 173.75 bu/ac, marking an increase of about 4.13% over the integrated method. These results underscore the efficacy of precision agriculture techniques in enhancing crop yields beyond traditional farming methods.

The financial implications of the observed yield enhancement are significant. For the wheat field size of 3.36 acres, the methodology led to an additional revenue of potentially $194.27, given the prevailing market price of $7 per bushel of wheat [111]. This translates to a savings of potentially $57.82 per acre, highlighting the economic efficacy of the approach. When extrapolating these findings to a larger scale, such as a field spanning 1,000 acres, the projected additional revenue is estimated to be potentially $57,817.48. This consistent per-acre savings further emphasizes the potential financial benefits and scalability of the methodology.

In the case of the corn field, the integrated method's baseline yield was 166.86 bu/ac. With the field size of 135.54 acres and a market price of $4.95 per bushel of corn [3], [89], the alternative strategies yielded the following increases: the farmer's approach, with a yield of 165.84 bu/ac, actually produced 1.02 bu/ac less than the baseline, not an increase, the satellite-based approach an extra 5.68 bu/ac, and the drone-based method a further 6.89 bu/ac over the baseline. These increases equate to additional revenues of potentially $28.11 for the satellite-based approach, and $34.11 per acre for the drone-based approach. For the entire corn field, the total additional revenues are estimated at $3,808.47 for the satellite-based approach, and $4,615.72 for the drone-based method. If these methods were applied to a 1,000-acre field, the estimated additional revenues could reach $10,080.00, $28,110.00, and $34,110.00, respectively, showcasing the considerable financial gains that can be achieved with precision agriculture techniques.

In conclusion, this study highlights the benefits of adopting the novel agricultural methodology, including cost savings from reduced nitrogen applications, increased revenue from enhanced wheat yields, and positive environmental implications.

5 Conclusion

5.1 Summary of findings

This research explored a new agricultural method to optimize nitrogen use in wheat and corn farming. Key findings are summarized below:

- **Wheat Field Findings (3.36 acres):**
  - *Nitrogen Reduction:* Achieved a 16.2% reduction in nitrogen application.
  - *Cost Savings:* Resulted in a saving of $26.45 for the field. Extrapolated to a 1,000-acre field, the savings could be potentially $7,870.00.
  - *Yield Increase:* Observed a yield of 75.09 bu/ac compared to 66.61 bu/ac in the control field, a 12.40% increase.
  - *Revenue Increase:* This increased yield led to an additional revenue of $194.27 for the field, equating to $57.82 per acre. For a 1,000-acre field, this could mean an additional $57,817.48.
  - *Statistical Significance:* T-tests and Cohen's d effect sizes indicated statistically significant differences, particularly in Zone 1 (Green zone).
  - *NUE:* The NUE showed a 16.2% increase compared to the control field, demonstrating the effectiveness of the optimized nitrogen application strategy.
- **Corn Field Findings (135.54 acres):**
  - *Nitrogen Reduction:* A 10% reduction in nitrogen application was implemented.
  - *Cost Savings:* Resulted in a saving of $491.25 for the field. Extrapolated to a 1,000-acre field, the savings could be potentially $3,624.40.

- *Yield Increase:* The approach suggested a yield of 173.75 bu/ac, compared to the traditional yield of 165.84 bu/ac, indicating a potential increase of 7.91 bu/ac, which is approximately a 4.77% increase.
- *Financial Impact:* This yield increase could lead to an additional revenue of approximately $39.15 per acre, significantly enhancing the overall profitability.
- *NUE:* Our approach suggests a 4.3% higher NUE in the corn field compared to the farmer's traditional nitrogen application rate, indicating a more efficient use of nitrogen in our methodology.

5.2 Implications and contributions

The findings contribute to discussions on sustainable and efficient agricultural practices. The method aligns with precision agriculture goals and suggests a need to re-evaluate traditional nitrogen application practices.

5.3 Considerations and future directions

This study has demonstrated that a precise determination of plants' nitrogen needs can lead to increased yield while reducing fertilizer usage, offering both cost savings and environmental benefits. Looking ahead, an important area of future work involves the development of an accessible digital tool. Envisioned as a mobile app, web service, or computer software, this tool would act as a recommendation system. It would take into account various factors such as field information, soil characteristics, and other relevant data to establish management zones, identify optimal locations for N-rich spots, and utilize remote sensing data (either provided by the farmer or automatically sourced from satellites) to create prescription maps for optimizing NUE. This proposed solution aims to translate the research findings into a practical application, making it accessible and easy to use for farmers without a scientific background, thus enabling them to enhance nitrogen use efficiency in their fields.

Continuing this line of research, it is crucial to explore the effects of this nitrogen optimization method on different crops and in diverse geographical settings. Furthermore, understanding its long-term impact on soil health, crop quality, and environmental sustainability remains a vital component of future studies. This approach not only aligns with the goals of sustainable agriculture but also opens up new possibilities for technological integration in farming practices.

5.4 Conclusion

This thesis introduced a novel agricultural method that brings both economic and environmental benefits, aligning with sustainable practices. The research lays the groundwork for future investigations and applications in precision agriculture, emphasizing the importance of considering both economic gains and environmental well-being.

REFERENCES

[1] V. I. Adamchuk, J. W. Hummel, M. T. Morgan, and S. K. Upadhyaya, "On-the-go soil sensors for precision agriculture," *Computers and electronics in agriculture*, vol. 44, no. 1, pp. 71–91, 2004.

[2] G. Agegnehu, D. Abera, G. Desta, and A. Rooyen, "Current innovations in making site specific nutrient management," 2023.

[3] AgriNews, *Corn price rises, soybeans unchanged*, https://www.agrinews-pubs.com/2023/11/01/corn-price-rises-soybeans-unchanged/, Accessed: 2023-11-09, 2023.

[4] Y. Akkem, S. K. Biswas, and A. Varanasi, "Smart farming using artificial intelligence: A review," *Engineering Applications of Artificial Intelligence*, vol. 120, p. 105 899, 2023.

[5] M. Alonso-Ayuso, J. Gabriel, and M Quemada, "Nitrogen use efficiency and residual effect of fertilizers with nitrification inhibitors," *European Journal of Agronomy*, vol. 80, pp. 1–8, 2016.

[6] F. Argento, T. Anken, F. Abt, E. Vogelsanger, A. Walter, and F. Liebisch, "Site-specific nitrogen management in winter wheat supported by low-altitude remote sensing and soil data," *Precision Agriculture*, vol. 22, pp. 364–386, 2021.

[7] S. Ayadi, S. Jallouli, Z. Chamekh, *et al.*, "Variation of grain yield, grain protein content and nitrogen use efficiency components under different nitrogen rates in mediterranean durum wheat genotypes," *Agriculture*, vol. 12, no. 7, p. 916, 2022.

[8] E. Baggs, R. M. Rees, K. Smith, and A. Vinten, "Nitrous oxide emission from soils after incorporating crop residues," *Soil use and management*, vol. 16, no. 2, pp. 82–87, 2000.

[9] *Balancing productivity and sustainability in agriculture*, Accessed: 2023-11-01, 2020. [Online]. Available: https://www.fao.org/sustainability/news/detail/en/c/1278123/.

[10] J. G. A. Barbedo, "Data fusion in agriculture: Resolving ambiguities and closing data gaps," *Sensors*, vol. 22, no. 6, p. 2285, 2022.

[11] S. Bauder and A. Varenhorst. "Check your bins this spring." Accessed: 09/01/2023. (2023), [Online]. Available: https://extension.sdstate.edu/check-your-bins-spring.

[12] F Berendse and R Aerts, *Nitrogen-use-efficiency: A biologically meaningful definition?* 1987.

[13] B. Boincean, D. Dent, B. Boincean, and D. Dent, "Tillage and conservation agriculture," *Farming the Black Earth: Sustainable and Climate-Smart Management of Chernozem Soils*, pp. 125–149, 2019.

[14] R. Bongiovanni and J. Lowenberg-DeBoer, "Precision agriculture and sustainability," *Precision agriculture*, vol. 5, no. 4, pp. 359–387, 2004.

[15] H. E. Bouis, C. Hotz, B. McClafferty, J. V. Meenakshi, and W. H. Pfeiffer, "Biofortification: A new tool to reduce micronutrient malnutrition," *Food and Nutrition Bulletin*, vol. 32, no. 1_suppl1, S31–S40, 2011.

[16] A. Bouwman, A. Beusen, J Griffioen, *et al.*, "Global trends and uncertainties in terrestrial denitrification and n2o emissions," *Philosophical Transactions of the Royal Society B: Biological Sciences*, vol. 368, no. 1621, p. 20 130 112, 2013.

[17] A. Bouwman, D. Lee, W. Asman, F. Dentener, K. Van Der Hoek, and J. Olivier, "A global high-resolution emission inventory for ammonia," *Global Biogeochemical Cycles*, vol. 11, no. 4, pp. 561–587, 1997.

[18] C. N. Boyer, B Wade Brorsen, J. B. Solie, and W. R. Raun, "Profitability of variable rate nitrogen application in wheat production," *Precision Agriculture*, vol. 12, pp. 473–487, 2011.

[19] K. G. Cassman, A. Dobermann, and D. T. Walters, "Agroecosystems, nitrogen-use efficiency, and nitrogen management," *AMBIO: A Journal of the Human Environment*, vol. 31, no. 2, pp. 132–140, 2002.

[20] B. Chen, E. Liu, Q. Tian, C. Yan, and Y. Zhang, "Soil nitrogen dynamics and crop residues. a review," *Agronomy for sustainable development*, vol. 34, pp. 429–442, 2014.

[21] I. A. Ciampitti and T. J. Vyn, "Physiological perspectives of changes over time in maize yield dependency on nitrogen uptake and associated nitrogen efficiencies: A review," *Field Crops Research*, vol. 133, pp. 48–67, 2012.

[22] *Climate Change 2014–Impacts, Adaptation and Vulnerability: Regional Aspects*. Cambridge University Press, 2014.

[23] D. L. Corwin and S. M. Lesch, "Protocols and guidelines for field-scale measurement of soil salinity distribution with eca-directed soil sampling," *Journal of Environmental and Engineering Geophysics*, vol. 18, no. 1, pp. 1–25, 2013.

[24] D. Coskun, D. T. Britto, W. Shi, and H. J. Kronzucker, "Nitrogen transformations in modern agriculture and the role of biological nitrification inhibition," *Nature Plants*, vol. 3, no. 6, pp. 1–10, 2017.

[25] *Cover crops for climate resilience*, Accessed: 2023-11-25, USDA Climate Hubs, 2023. [Online]. Available: https://www.climatehubs.usda.gov/hubs/international/topic/cover-crops-climate-resilience.

[26] S. De Baets, J. Poesen, J. Meersmans, and L Serlet, "Cover crops and their erosion-reducing effects during concentrated flow erosion," *Catena*, vol. 85, no. 3, pp. 237–244, 2011.

[27] H. Di and K. Cameron, "Nitrate leaching in temperate agroecosystems: Sources, factors and mitigating strategies," *Nutrient cycling in agroecosystems*, vol. 64, pp. 237–256, 2002.

[28] M. Diacono, P. Rubino, and F. Montemurro, "Precision nitrogen management of wheat. a review," *Agronomy for Sustainable Development*, vol. 33, pp. 219–241, 2013.

[29] J. Diamond, *Guns, germs, and steel: The fates of human societies*. W. W. Norton & Company, 1997.

[30] Y. Du, T. Li, and B. He, "Runoff-related nutrient loss affected by fertilization and cultivation in sloping croplands: An 11-year observation under natural rainfall," *Agriculture, Ecosystems & Environment*, vol. 319, p. 107 549, 2021.

[31] D Ehlert, J Schmerler, and U Voelker, "Variable rate nitrogen fertilisation of winter wheat based on a crop density sensor," *Precision Agriculture*, vol. 5, pp. 263–273, 2004.

[32] B. Eichler-Löbermann, P. Köhne, S. Kowalski, and A. Schnug, "Effect of catch cropping on phosphorus bioavailability in comparison to organic and inorganic fertilization," *Journal of Plant Nutrition and Soil Science*, vol. 173, no. 3, pp. 353–358, 2010.

[33] K. Ennouri, S. Smaoui, Y. Gharbi, *et al.*, "Usage of artificial intelligence and remote sensing as efficient devices to increase agricultural system yields," *Journal of Food Quality*, vol. 2021, pp. 1–17, 2021.

[34] N. K. Fageria and V. Baligar, "Enhancing nitrogen use efficiency in crop plants," *Advances in agronomy*, vol. 88, pp. 97–185, 2005.

[35] S. Farzadfar, J. D. Knight, and K. A. Congreves, "Soil organic nitrogen: An overlooked but potentially significant contribution to crop nutrition," *Plant and Soil*, vol. 462, pp. 7–23, 2021.

[36] D. D. Fromme, D. L. Coker, M. L. McFarland, *et al.*, "Residual soil nitrogen credits for corn production along the upper texas gulf coast region," *Journal of Plant Nutrition*, vol. 40, no. 1, pp. 23–32, 2017.

[37] C Ganeshkumar, S. K. Jena, A Sivakumar, and T Nambirajan, "Artificial intelligence in agricultural value chain: Review and future directions," *Journal of Agribusiness in Developing and Emerging Economies*, vol. 13, no. 3, pp. 379–398, 2023.

[38] P. Garbeva, E. M. Baggs, and J. I. Prosser, "Phylogeny of nitrite reductase (nirk) and nitric oxide reductase (norb) genes from nitrosospira species isolated from soil," *FEMS microbiology letters*, vol. 266, no. 1, pp. 83–89, 2007.

[39] T. Garnett, M. Appleby, A. Balmford, *et al.*, "Agriculture. sustainable intensification in agriculture: Premises and policies," *Science*, vol. 341, no. 6141, pp. 33–34, 2009.

[40] R. Girshick, "Fast r-cnn," in *Proceedings of the IEEE international conference on computer vision*, 2015, pp. 1440–1448.

[41] B Halling-Sørensen *et al.*, "Process chemistry and biochemistry of denitrification.," *The removal of nitrogen compounds from wastewater.*, pp. 119–151, 1993.

[42] H.-l. HAO, Y.-z. WEI, X.-e. YANG, F. Ying, and C.-y. WU, "Effects of different nitrogen fertilizer levels on fe, mn, cu and zn concentrations in shoot and grain quality in rice (oryza sativa)," *Rice Science*, vol. 14, no. 4, pp. 289–294, 2007.

[43] M. Hawkesford, "Reducing the reliance on nitrogen fertilizer for wheat production," *Journal of Cereal Science*, vol. 59, no. 3, pp. 276–283, 2014.

[44] M. Hawkesford and P. Barraclough, "The molecular physiology of nutrient transport across the plasma membrane of plant cells," *Annual Plant Reviews online*, vol. 15, pp. 133–162, 2012.

[45] G. He, X. Liu, and Z. Cui, "Achieving global food security by focusing on nitrogen efficiency potentials and local production," *Global Food Security*, vol. 29, p. 100 536, 2021.

[46] P. B. Hegedus, S. A. Ewing, C. Jones, and B. D. Maxwell, "Using spatially variable nitrogen application and crop responses to evaluate crop nitrogen use efficiency," *Nutrient Cycling in Agroecosystems*, vol. 126, no. 1, pp. 1–20, 2023.

[47] *How cover crops reduce nitrogen input and improve soil health*, Accessed: 2023-11-25, LSU AgCenter, 2023. [Online]. Available: https://www.lsuagcenter.com/profiles/lbenedict/articles/page1609799041027.

[48] *Immobilization and mineralization of nitrogen in agricultural soils*, Accessed: 2023-11-25, Penn State Extension, 2023. [Online]. Available: https://extension.psu.edu/immobilization-and-mineralization-of-nitrogen-in-agricultural-soils.

[49] Iowa State University Extension and Outreach, *Nitrogen losses after heavy rains*, Integrated Crop Management, Accessed: [insert date here]. [Online]. Available: https://crops.extension.iastate.edu/encyclopedia/nitrogen-losses-after-heavy-rains.

[50] J. Jiang, Y. Wu, Q. Liu, *et al.*, "Developing an efficiency and energy-saving nitrogen management strategy for winter wheat based on the uav multispectral imagery and machine learning algorithm," *Precision Agriculture*, pp. 1–25, 2023.

[51] L. Jiang, G. Ball, C. Hodgman, A. Coules, H. Zhao, and C. Lu, "Analysis of gene regulatory networks of maize in response to nitrogen," *Genes*, vol. 9, no. 3, p. 151, 2018.

[52] C. Jones and K. Olson-Rutz, "Practices to increase wheat grain protein," *Montana State University Extension*, 2012.

[53] S. Kang, L. Zhang, X. Song, *et al.*, "Runoff and sediment loss responses to rainfall and land use in two agricultural catchments on the loess plateau of china," *Hydrological Processes*, vol. 15, no. 6, pp. 977–988, 2001.

[54] M. Khanna, S. S. Atallah, S. Kar, *et al.*, "Digital transformation for a sustainable agriculture in the united states: Opportunities and challenges," *Agricultural Economics*, vol. 53, no. 6, pp. 924–937, 2022.

[55] S. C. Killpack and D. Buchholz, "Nitrogen in the environment: Ammonia volatilization," 1993.

[56] N. Kitchen, S. Drummond, E. Lund, K. Sudduth, and G. Buchleiter, "Soil electrical conductivity and topography related to yield for three contrasting soil–crop systems," *Agronomy journal*, vol. 95, no. 3, pp. 483–495, 2003.

[57] S. Kuchta, D. Neilsen, T. Forge, B. J. Zebarth, and C. Nichol, "Nitrogen, irrigation, and alley management effects on nitrate leaching from raspberry," *Vadose Zone Journal*, vol. 19, no. 1, e20054, 2020.

[58] C. Kumar, P. Mubvumba, Y. Huang, J. Dhillon, and K. Reddy, "Multi-stage corn yield prediction using high-resolution uav multispectral data and machine learning models," *Agronomy*, vol. 13, no. 5, p. 1277, 2023.

[59] M. Langholtz, B. H. Davison, H. I. Jager, *et al.*, "Increased nitrogen use efficiency in crop production can provide economic and environmental benefits," *Science of the Total Environment*, vol. 758, p. 143 602, 2021.

[60] L. Lassaletta, G. Billen, B. Grizzetti, J. Anglade, and J. Garnier, "50 year trends in nitrogen use efficiency of world cropping systems: The relationship between yield and nitrogen input to cropland," *Environmental Research Letters*, vol. 9, no. 10, p. 105 011, 2014.

[61] L. Lassaletta, R. Einarsson, and M. Quemada, "Nitrogen use efficiency of tomorrow," *Nature Food*, pp. 1–2, 2023.

[62] F Li, Y Miao, F Zhang, *et al.*, "In-season optical sensing improves nitrogen-use efficiency for winter wheat," *Soil Science Society of America Journal*, vol. 73, no. 5, pp. 1566–1574, 2009.

[63] A. Lodhi, M Arshad, F Azam, M. Sajjad, and M Ashraf, "Changes in mineral and mineralizable n of soil incubated at varying salinity, moisture and temperature regimes," *Pak. J. Bot*, vol. 41, no. 2, pp. 967–980, 2009.

[64] U. K. Mandal, K. Sharma, J. Prasad, *et al.*, "Nutrient losses by runoff and sediment from an agricultural field in semi-arid tropical india," *Indian Journal of Dryland Agricultural Research and Development*, vol. 27, no. 1, pp. 1–9, 2012.

[65] V. Manjula, "Soils, plant nutrition and nutrient management," *Soil Testing and Plant Diagnostic Service Laboratory.(Provide page number)*, 2009.

[66] F. Mariotti, D. Tomé, and P. P. Mirand, "Converting nitrogen into protein—beyond 6.25 and jones' factors," *Critical reviews in food science and nutrition*, vol. 48, no. 2, pp. 177–184, 2008.

[67] C. Masclaux-Daubresse, F. Daniel-Vedele, J. Dechorgnat, F. Chardon, L. Gaufichon, and A. Suzuki, "Nitrogen uptake, assimilation and remobilization in plants: Challenges for sustainable and productive agriculture," *Annals of botany*, vol. 105, no. 7, pp. 1141–1157, 2010.

[68] S. McGinn, H. Janzen, T. Coates, K. Beauchemin, and T. Flesch, "Ammonia emission from a beef cattle feedlot and its local dry deposition and re-emission," *Journal of Environmental Quality*, vol. 45, no. 4, pp. 1178–1185, 2016.

[69] D. McKay Fletcher, S. Ruiz, K. Williams, *et al.*, "Projected increases in precipitation are expected to reduce nitrogen use efficiency and alter optimal fertilization timings in agriculture in the south east of england," *ACS Es&t Engineering*, vol. 2, no. 8, pp. 1414–1424, 2022.

[70] R. H. Moll, E. J. Kamprath, and W. A. Jackson, "Analysis and interpretation of factors which contribute to efficiency of nitrogen utilization," *Agronomy journal*, vol. 74, no. 3, pp. 562–564, 1982.

[71] F Morari, V Zanella, S Gobbo, *et al.*, "Coupling proximal sensing, seasonal forecasts and crop modelling to optimize nitrogen variable rate application in durum wheat," *Precision Agriculture*, vol. 22, pp. 75–98, 2021.

[72] D. J. Mulla, "Twenty five years of remote sensing in precision agriculture: Key advances and remaining knowledge gaps," *Biosystems Engineering*, vol. 114, no. 4, pp. 358–371, 2013. DOI: 10.1016/j.biosystemseng.2012.08.009.

[73] P. Nardi, H. J. Laanbroek, G. W. Nicol, *et al.*, "Biological nitrification inhibition in the rhizosphere: Determining interactions and impact on microbially mediated processes and potential applications," *FEMS Microbiology Reviews*, vol. 44, no. 6, pp. 874–908, 2020.

[74] National Research Council (US) Subcommittee on the Tenth Edition of the Recommended Dietary Allowances, *Recommended Dietary Allowances: 10th Edition*. Washington (DC): National Academies Press (US), 1989, ch. 6. [Online]. Available: https://www.ncbi.nlm.nih.gov/books/NBK234922/.

[75] U. Nations. "Global issues: Population." (n.d.), [Online]. Available: https://www.un.org/en/global-issues/population.

[76] B. Pan, L. Xia, S. K. Lam, *et al.*, "A global synthesis of soil denitrification: Driving factors and mitigation strategies," *Agriculture, Ecosystems & Environment*, vol. 327, p. 107 850, 2022.

[77] Penn State Extension, *Immobilization and mineralization of nitrogen in agricultural soils*, https://extension.psu.edu/immobilization-and-mineralization-of-nitrogen-in-agricultural-soils, [Online; accessed 27-Nov-2023], 2023.

[78] F. J. Pierce and P. Nowak, "Aspects of precision agriculture," in *Advances in agronomy*. Academic Press, 1999, vol. 67, pp. 1–85.

[79] J. J. Pignatello and S. L. Nason, "Importance of soil properties and processes on bioavailability of organic compounds," *Bioavailability of Organic Chemicals in Soil and Sediment*, pp. 7–41, 2020.

[80] M Quemada and M. Cabrera, "Ceres-n model predictions of nitrogen mineralized from cover crop residues," *Soil Science Society of America Journal*, vol. 59, no. 4, pp. 1059–1065, 1995.

[81] D. Radočaj, M. Jurišić, and M. Gašparović, "The role of remote sensing data and methods in a modern approach to fertilization in precision agriculture," *Remote Sensing*, vol. 14, no. 3, p. 778, 2022.

[82] D. Radočaj, I. Plaščak, and M. Jurišić, "Global navigation satellite systems as state-of-the-art solutions in precision agriculture: A review of studies indexed in the web of science," *Agriculture*, vol. 13, no. 7, p. 1417, 2023.

[83] T. Ranatunga, K. Hiramatsu, T. Onishi, and Y. Ishiguro, "Process of denitrification in flooded rice soils," *Reviews in Agricultural Science*, vol. 6, pp. 21–33, 2018.

[84] T. O. Randhir and J. G. Lee, "Designing spatial incentives to manage agricultural nonpoint source pollution," Paper presented at AAEA annual meeting in Toronto, Canada, 1997.

[85] N. N. Ranells and M. G. Wagger, "Nitrogen-15 recovery and release by rye and crimson clover cover crops," *Soil Science Society of America Journal*, vol. 61, no. 3, pp. 943–948, 1997.

[86] W. R. Raun, J. B. Solie, G. V. Johnson, *et al.*, "Improving nitrogen use efficiency in cereal grain production with optical sensing and variable rate application," *Agronomy Journal*, vol. 94, no. 4, pp. 815–820, 2002.

[87] N. Rawal, K. R. Pande, R. Shrestha, and S. P. Vista, "Nutrient use efficiency (nue) of wheat (triticum aestivum l.) as affected by npk fertilization," *Plos one*, vol. 17, no. 1, e0262771, 2022.

[88] S. Ren, K. He, R. Girshick, and J. Sun, "Faster r-cnn: Towards real-time object detection with region proposal networks," *Advances in neural information processing systems*, vol. 28, 2015.

[89] Reuters, *Grains-corn futures backpedal from august high, end below $5 a bushel*, https://www.reuters.com/article/global-grains/grains-corn-futures-backpedal-from-august-high-end-below-5-a-bushel-idUSL1N2Z21UQ, Accessed: 2023-11-09, 2023.

[90] M. Reynolds, *Application of physiology in wheat breeding*. Cimmyt, 2001.

[91] W. Riley, I Ortiz-Monasterio, and P. Matson, "Nitrogen leaching and soil nitrate, nitrite, and ammonium levels under irrigated wheat in northern mexico," *Nutrient Cycling in Agroecosystems*, vol. 61, pp. 223–236, 2001.

[92] R. Roberts, B. English, and S. Mahajanashetti, "Evaluating the returns to variable rate nitrogen application," *Journal of Agricultural and Applied Economics*, vol. 32, no. 1, pp. 133–143, 2000.

[93] C. F. Runge and B. Senauer, "How biofuels could starve the poor," *Foreign Affairs*, vol. 86, no. 3, pp. 41–53, 2007.

[94] D. Schimmelpfennig, "Farm profits and adoption of precision agriculture," U.S. Department of Agriculture, Economic Research Service, Tech. Rep. ERR-217, 2016.

[95] S. Schlüter, C. Großmann, J. Diel, *et al.*, "Long-term effects of conventional and reduced tillage on soil structure, soil ecological and soil hydraulic properties," *Geoderma*, vol. 332, pp. 10–19, 2018.

[96] G. Schnitkey, N. Paulson, C. Zulauf, and J. Baltz, "Nitrogen fertilizer prices stabilize at high levels in spring 2023," *farmdoc daily*, vol. 13, no. 108, 2023.

[97] SDSU Extension, *Leveling the playing field for u.s. corn*, Accessed: 2023-11-07, 2023. [Online]. Available: https://extension.sdstate.edu/leveling-playing-field-us-corn.

[98] B. Sharma and R. Ahlert, "Nitrification and nitrogen removal," *Water Research*, vol. 11, no. 10, pp. 897–925, 1977.

[99] B. Shiferaw, B. M. Prasanna, J. Hellin, and M. Bänziger, "Crops that feed the world 6. past successes and future challenges to the role played by maize in global food security," *Food Security*, vol. 3, no. 3, pp. 307–327, 2011.

[100] H Shindo and T Nishio, "Immobilization and remineralization of n following addition of wheat straw into soil: Determination of gross n transformation rates by 15n-ammonium isotope dilution technique," *Soil Biology and Biochemistry*, vol. 37, no. 3, pp. 425–432, 2005.

[101] B. P. Singh, B. J. Hatton, B. Singh, A. L. Cowie, and A. Kathuria, "Influence of biochars on nitrous oxide emission and nitrogen leaching from two contrasting soils," *Journal of environmental quality*, vol. 39, no. 4, pp. 1224–1235, 2010.

[102] S. T. Sonka and K. F. Coaldrake, "Cyberfarm: What does it look like? what does it mean?" *Amer. J. Agr. Econ.*, vol. 78, pp. 263–268, 1996.

[103] S Stamatiadis, J. Schepers, E Evangelou, *et al.*, "Variable-rate nitrogen fertilization of winter wheat under high spatial resolution," *Precision Agriculture*, vol. 19, pp. 570–587, 2018.

[104] Strip-Till Farmer, *Nitrogen sensing for on-the-go variable rate application in corn*, Strip-Till Farmer, Accessed: [insert date here]. [Online]. Available: https://www.striptillfarmer.com/articles/1844-nitrogen-sensing-for-on-the-go-variable-rate-application-in-corn.

[105] M. A. Sutton, O. Oenema, J. W. Erisman, A. Leip, H. van Grinsven, and W. Winiwarter, "Too much of a good thing," *Nature*, vol. 472, no. 7342, pp. 159–161, 2011.

[106] *The state of agricultural commodity markets 2018: Agricultural trade, climate change and food security*. Rome, Italy: Food and Agriculture Organization of the United Nations, 2018.

[107] *The state of food and agriculture 2020: Overcoming water challenges in agriculture*. Rome, Italy: Food and Agriculture Organization of the United Nations, 2020.

[108] S. Thrikawala, A. Weersink, G. Kachanoski, and G. Fox, "Economic feasibility of variable-rate technology for nitrogen on corn," *Amer. J. Agr. Econ.*, vol. 81, pp. 914–927, 1999.

[109] D. Tilman, K. G. Cassman, P. A. Matson, R. Naylor, and S. Polasky, "Agricultural sustainability and intensive production practices," *Nature*, vol. 418, no. 6898, pp. 671–677, 2002.

[110] N. Tremblay, E. Fallon, and N. Ziadi, "Sensing of crop nitrogen status: Opportunities, tools, limitations, and supporting information requirements," *HortTechnology*, vol. 21, no. 3, pp. 274–281, 2011.

[111] United States Department of Agriculture, National Agricultural Statistics Service, *Prices received: Wheat prices received by month, us*, Accessed: 2023-10-31, 2023. [Online]. Available: https://www.nass.usda.gov/Charts_and_Maps/Agricultural_Prices/pricewh.php.

[112] University of California Agriculture and Natural Resources, *Top dressing wheat: Growing degree day models help optimize nitrogen application timing*, Sacramento Valley Field Crops - ANR Blogs, Accessed: 2023-11-13, 2023. [Online]. Available: https://ucanr.edu/blogs/blogcore/postdetail.cfm?postnum=48234.

[113] University of Minnesota Extension, *Understanding nitrogen in soils*, https://extension.umn.edu/nitrogen/understanding-nitrogen-soils, [Online; accessed 27-Nov-2023], 2023.

[114] *Usda economic research service - wheat and corn*, https://www.ers.usda.gov/, 2020.

[115] E. R. S. USDA. "Corn received the highest application rate of nitrogen from a manure source." (2023), [Online]. Available: https://www.ers.usda.gov/data-products/chart-gallery/gallery/chart-detail/?chartId=106252.

[116] X Wang, Y Miao, R Dong, G Mi, K Kusnierek, and W. Batchelor, "Combining crop growth modeling, active sensing and machine learning to improve in-season nitrogen management of maize," in *Precision agriculture'23*, Wageningen Academic Publishers, 2023, pp. 359–366.

[117] Y. Wang, W. Shi, and T. Wen, "Prediction of winter wheat yield and dry matter in north china plain using machine learning algorithms for optimal water and nitrogen application," *Agricultural Water Management*, vol. 277, p. 108 140, 2023.

[118] M. Waqas, M. J. Hawkesford, and C.-M. Geilfus, "Feeding the world sustainably: Efficient nitrogen use," *Trends in Plant Science*, 2023.

[119] B. B. Ward, D. J. Arp, and M. G. Klotz, *Nitrification*. Washington, DC: American Society for Microbiology Press, 2011, p. 454.

[120] *World Development Report 2021: Data for Better Lives*. Washington, DC: World Bank, 2021.

[121] A. Yassen, E. Abou El-Nour, and S Shedeed, "Response of wheat to foliar spray with urea and micronutrients," *Journal of American Science*, vol. 6, no. 9, pp. 14–22, 2010.

[122] J. Y. Ye, W. H. Tian, and C. W. Jin, "Nitrogen in plants: From nutrition to the modulation of abiotic stress adaptation," *Stress Biology*, vol. 2, no. 1, p. 4, 2022.

[123] V. Zelenev, A. Van Bruggen, P. Leffelaar, J Bloem, and A. Semenov, "Oscillating dynamics of bacterial populations and their predators in response to fresh organic matter added to soil: The simulation model 'bacwave-web'," *Soil Biology and Biochemistry*, vol. 38, no. 7, pp. 1690–1711, 2006.

[124] C. Zhang and J. M. Kovacs, "The application of small unmanned aerial systems for precision agriculture: A review," *Precision agriculture*, vol. 13, pp. 693–712, 2012.